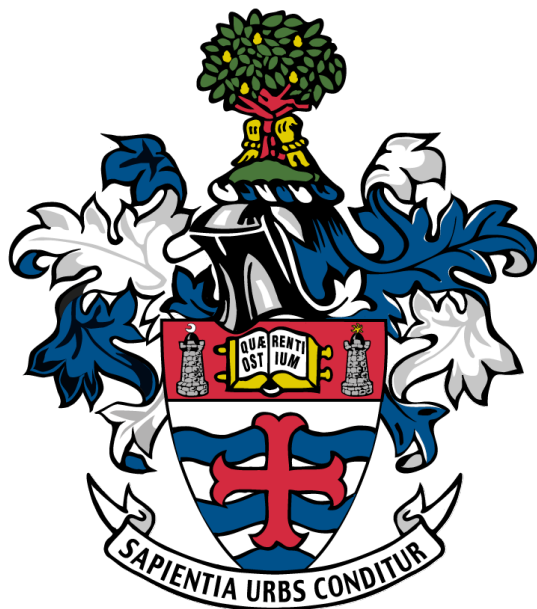


“Every good act of giving and every perfect gift is from above, coming down from the Father who made the heavenly lights; with him there is neither variation nor darkness caused by turning.”

James 1:17, CJB



Quantum dots as emitters for a chip integrated atom-photon interface

KADE MOCK & ROSHAN CHACKO

A thesis presented in fulfilment of the requirements for the degree of Master of Physics

Supervisor: Dr Lucia Hackermüller

School of Physics and Astronomy
University of Nottingham
Nottingham, England
May, 2022

TABLE OF CONTENTS

Acknowledgements	i
Abstract	ii
Chapter 1: Introduction	1
1.1 Basis	1
1.2 Aims and Objectives	1
Chapter 2: Background and Theory	3
2.1 Quantum Dots	3
2.1.1 Atomic Physics	3
2.1.2 Semiconductor Structure and Excitons	3
2.1.3 Species	6
2.1.4 Blinking	6
2.1.5 Single Photon Measurement and Anti-bunching	7
2.2 Optics	9
2.2.1 Lenses	9
2.2.2 Waveguides	10
2.2.3 Electromagnetic Waves	11
Chapter 3: Methodology and Results	12
3.1.2 Obtaining the imaging resolution	13
3.2.1 Preparing the samples	15
3.2.2 Spin Coating and microscope objective imaging	17
3.3 Coupling Mechanisms	20
3.3.1 Aspherical Lenses	20
3.3.2 Lensed Fibre & Butt-Coupler	21
Chapter 4: Discussion	25
4.1 Review of Imaging System	25
4.2 Review of Blinking Observations in Quantum Dots	26
4.3 Review of Coupling Mechanisms	27
Chapter 5: Outlook	30
4.4 Testing Single Photon Emission of Quantum Dots	30
4.5 Quantum Information Applications	31
Chapter 6: Conclusions	33
Bibliography	34

ACKNOWLEDGEMENTS

We wish to thank our project supervisor Dr Lucia Hackermüller for guidance and regular meetings throughout the course of this project. We also wish to extend a special thanks to all the staff and post-graduate students in the optics group for their input during our project, especially Dr Nathan Cooper who offered valuable insight into the technical details of our project.

ABSTRACT

The interface between coherent and sub-poissonian light sources and solid state devices is vitally important in quantum computing and quantum information applications. A primary motivation for this is the efficient transmission of the information contained within a photon from one position to another without obfuscating the quantum properties. In this report, we

investigate the possibility of coupling coherent light into waveguides on an optical chip developed during an EU led commision known as the ErbEStA project¹. The chip is designed for the integration of atomic quantum emitters such as quantum dots. Therefore, we also inspect and image CdSeS/ZnS alloyed quantum dots with various microscope objectives as well as a custom built microscope setup designed to image down to 5 μm in resolution. Fluorescence is observed from the quantum dots, and studied in detail, and initial steps we taken to integrate them into the waveguide cavity. We look to relevant literature to draw conclusions on how this could act as a reliable and scalable single photon source for quantum information applications.

CHAPTER 1: INTRODUCTION

Basis

In addition to the profound discoveries on the nature of the universe, quantum mechanics has also been realised in technologies ranging from semiconductor devices to lasers, utilising its theoretical aspects such as energy quantisation and wave-particle duality. These discoveries have become invaluable to everyday life, while a novel surge of research has transpired in parallel, investigating related phenomena such as: quantum superposition, entanglement, and quantum measurement. This is the field of quantum photonics, the study of the generation, detection and manipulation of light, with applications for quantum information science and quantum cryptography; proliferating the second quantum revolution².

There are three main foci³ that quantum photonics need to make advances in: fast and efficient photon counters, linear and non-linear photonic circuits, and single photon sources. It is possible for atoms, ions and organic molecules to be single photon sources, however, their low collection efficiency of photons and their poor photostability cajole the research to look for solutions in solid state systems.

To have a device capable of reliable photon output, it must overcome the intrinsically quantum nature of single photon emission and coupling. Cold atoms and quantum dots are two materials which can produce the sub-poissonian photon output distribution required for regulated single photon emission, though the methods of doing so vary⁴⁵⁶. For cold atoms, the premier method of producing single photon emission is via a rydberg blockade. While for quantum dots, injection into a waveguide cavity is chosen. Both methods work to increase the coupling efficiency of photons into the correct waveguide (quantum) mode.

Furthermore, it's important to consider what purpose a single photon source might be used for. Quantum applications such as computing and information transfer will ideally be as small as possible while maintaining powerful properties. As a result, a waveguide which carries light from one position to another is used because they are easily miniaturised and subsequently, will not bottleneck the size of quantum devices in the future.

Aims and Objectives

The main aim of the project was to evaluate an optical chip as an effective atom-photon interface by using quantum dots as the experimental atomic quantum emitters. The optical chip was designed during the ErBeSta project¹, and its schematic is shown in Figure 1:

As stated, our main task was to explore the possibility and limiting factors surrounding the coupling of light into the waveguides on the chip. To accomplish this, a bespoke microscope imaging device was built then tested using an array of lenses. A Thorlabs CCD sensor was always used as the digital interface. Details about the performance of different focal lengths and positions of various lenses were compared.

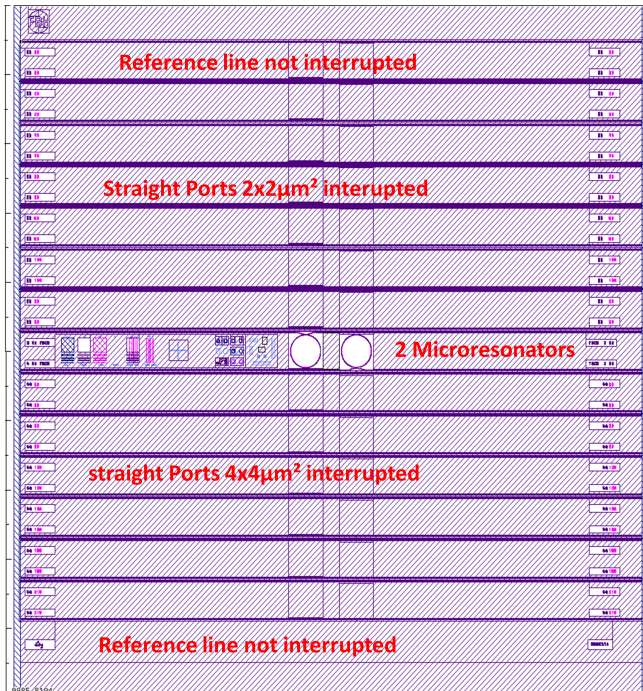


Figure 1: This is a schematic of the optical chip created during the Erbesta project which was EU commisioned project. The chip contains waveguides (shown by the dark purple ridges) that were manufactured using optical lithography, and ports between the waveguides allow for the integration of atomic emitters such as quantum dots.

After developing the imaging system and testing it against a calibration plate to measure the resolution of the device, we used the system to complete the objective of imaging individual colloidal quantum dots. In specific CdSeS/ZnS alloyed quantum dots were chosen for their emission wavelength, which was similar to the wavelength of light the waveguide was designed to accept. Using a dichroic mirror it is also be possible to eliminate the light incident on the quantum dots. With the overall goal being to couple light emitted from the quantum dots into the waveguide tracks.

Before attempting to couple light from the quantum dots into the waveguide, we also intended to couple light from a laser source into the waveguide, this aim was outlined as it would provide valuable insight into the methods used for coupling so that we could mimic the procedure for what we anticipated would be a significantly more difficult process, as there would be no way to easily align the quantum dots with the waveguide chip.

The last goal was to measure the transmittance of the light while performing the coupling, with and without quantum dots. Measuring the transmittance would serve the purpose of determining where power is being lost in the system and as a result attempt to improve the efficiency by adjusting the coupling in the location causing losses.

CHAPTER 2: BACKGROUND AND THEORY

Quantum Dots

Atomic Physics

Atomic physics is the most fundamental physics that underpins all the further information discussed in this report. Before attempting to understand quantum dots, the atom-photon interface and how to produce coupling within a waveguide, it is important to briefly review the atomic physics that are being mimicked and exploited by quantum dots. Most importantly to our investigation is the structure of the atom, and the energy levels of the electrons confined within it. Electrons may only occupy discrete states called energy levels. An electron can transition from the ground state to a number of excited states, depending on how much energy was provided in the initial excitement. This excitement is brief and the electron will return to the ground state shortly after being excited. The time scale on which this occurs is directly related to the Heisenberg uncertainty principle, whereby:

$$\sigma_x \sigma_p \geq \frac{\hbar}{2} \quad (1)$$

Where σ_x is the position uncertainty, σ_p is the momentum uncertainty and \hbar is the reduced planck constant. An equivalent form may present a more adequate explanation for how this impacts the lifetime of an electron in an excited state:

$$\sigma_E \sigma_t \geq \frac{\hbar}{2} \quad (2)$$

Where σ_E is the energy uncertainty and σ_t is the lifetime uncertainty⁷. As a result of this drop in energy, the process will release a photon, equal in energy to the gap between the energy level transition that just occurred.

$$\Delta E = hf \quad (3)$$

where ΔE is the difference in energy between the two levels, h is Planck's constant, and f is the frequency of the photon produced.

Semiconductor Structure and Excitons

Similarly to the atomic physics discussed above, semiconductor structure is also very fundamental physics which dictates the behaviour of quantum dots. The most simple definition of a semiconductor is a material which has a variable resistivity based upon some external factor such as: Temperature, light intensity or strain. There are two types of semiconductor materials that are generally used in commercial and scientific applications: Intrinsic semiconductors and Extrinsic semiconductors⁸. Intrinsic semiconductors are materials such as silicon which have an equal number of electrons and holes. Extrinsic semiconductors on the other hand, are materials such as gallium or arsenic. These materials have an unequal amount of electrons and holes, subdivided into p-type and n-type semiconductors; n-type have an abundance of

electrons, while p-type have an abundance of holes⁸.

Not only can semiconductors be characterised by the content of their charge carriers, but they may also be characterised by the type of band gap they exhibit. The band gap in a semiconductor is the difference in energy between the top of the valence band and the bottom of the conduction band. There are two types of band gap: Direct band gap and indirect band gap. A direct band gap semiconductor contains a maximum in the valence band at the same position in momentum space as the minimum in the conduction band.

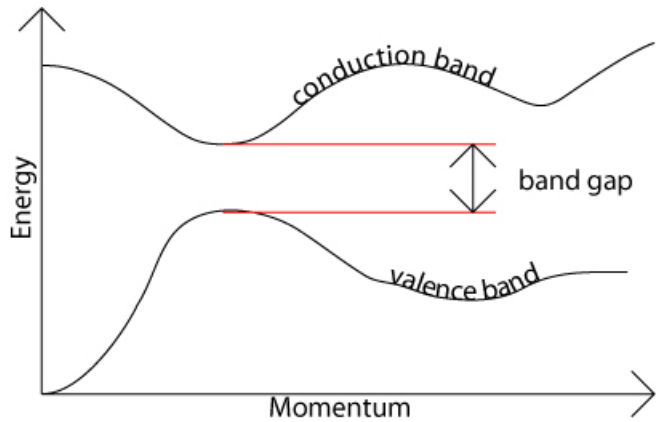


Figure 2: An illustration of the energy gap exhibited by direct band semiconductors in momentum space⁹.

Moreover, indirect band gap semiconductors contain a maximum in the valance band at a different position in momentum space than the minimum in the conduction band.

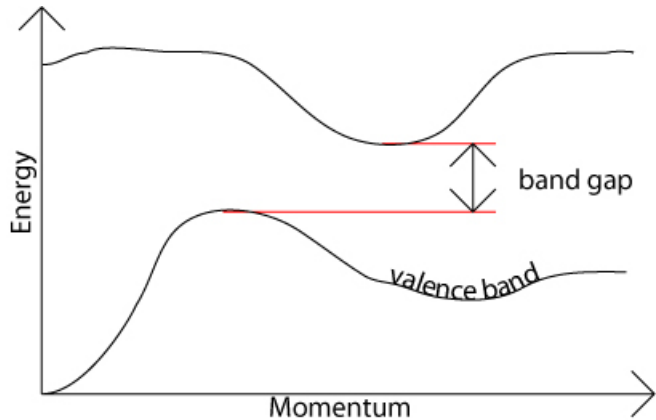


Figure 3: An illustration of the energy gap exhibited by indirect band gap semiconductor in momentum space⁹.

As a result of this misalignment in momentum space, for a photon with energy equivalent to the band gap energy to induce an excitation in an indirect band gap semiconductor, the electron must also gain (or lose) momentum by interacting with the lattice vibrations within the bulk semiconductor. In essence the electron must interact with both a photon and a phonon to be raised to the conduction band. Since the band peaks occur at the same position in momentum space, electrons excited within this type of structure have no need to interact with phonons and as a result are far more consistent emitters (especially at lower temperatures) than their

indirect band gap counterparts¹⁰.

Quantum dots, also known as artificial atoms, are semiconductor structures containing multiple atoms on the scale of tens to thousands of atoms per quantum dot. These structures are vitally useful in quantum mechanics as they restrict the quantisation of energy levels far beyond that of a regular semiconductor material¹¹. As a result of this confinement, we can produce effects such as antibunching, which produces streams of photons in a uniquely uniform manner. This property can be manipulated to produce photon emitters which exhibit coherence, where the temporal and spacial components of the photon are coherent with other photons from the source¹².

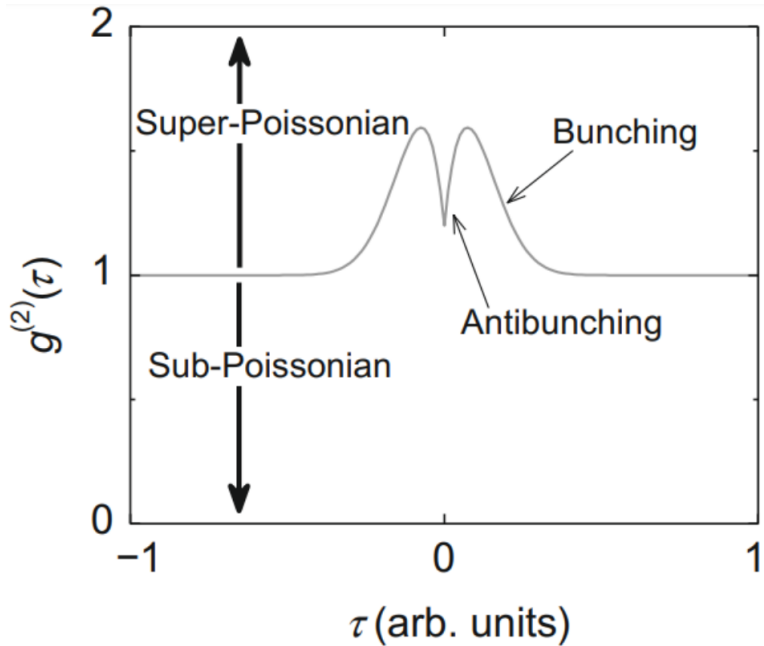


Figure 4: The figure shows local antibunching around $\tau \approx 0$. This function will often appear in real data, as the photon emission tends to bunch causing resonances. This leads to many bunching peaks. The dip which is characteristic of antibunching (labelled) will only appear around the resonant peak at $\tau \approx 0$, all other peaks will follow a poissonian distribution¹³

It is also worth noting that it is not electrons which move between the highly quantised energy levels of the quantum dot, instead it is the exciton a multi-particle structure containing an electron and a hole. The confinement within quantum dots allow highly predictable energy levels where excitons may form and recombine, mimicking the excited state and ground state of electron energy levels within atoms¹³. This exciton recombination is the phenomenon that produces photons as a bi-product of the process, leading to the highly desirable effects such as anti-bunching.

In addition to this, the electron and hole ground states of a QD exhibit twofold spin degeneracy, the degenerate levels are: (111), (121), (211), and (221), where the quantum numbers in brackets are associated with the confinement along x, y, and z. Thus, the recombination can produce both excitonic and biexcitonic emissions, and these are further split into polarised doubles¹⁴. Various factors affect the size of the splitting, including QD

size, shape, and chemical composition. This is what makes QDs ‘artificial atoms’, and enables them to be excellent emitters and therefore very good single-photon sources.

Species

As discussed, quantum dots are incredibly useful materials in photonics and quantum technology. There are two categories of quantum dots: Self-assembled (epitaxial) and colloidal. The main difference is the method of production and the phase of the quantum dots¹⁵. For brevity I will focus mainly on colloidal quantum dots, because this type is far easier to integrate into waveguide cavities due to their liquid phase. Colloidal quantum dots can be fabricated via plasma synthesis and typically exist as binary compounds, with most popular combinations being of group III and V atoms. Specifically III-Nitride compounds are overwhelmingly used in the literature in recent years due to promising application as photodiodes, single photon emitters and quantum dot lasers^{16 17 18}. More recently there have also been developments for colloidal perovskite quantum dots, which are highly desirable because they show promise for applications as a wavelength tunable laser, and show strong photon anti-bunching at room temperatures¹⁹.

As we will discuss later the primary disadvantage of using colloidal quantum dots is due to photoluminescence intermittency. Self-assembled quantum dots do not exhibit this property and are far more stable. Despite this they have problems of their own. Most prominent of which are the difficulties associated with growing isolated quantum dots and lack of versatility integrating these dots into scalable semiconductor devices; where self-assembled dots often have to be fabricated into bespoke devices rather than deposited in premade devices²⁰. Self-assembled quantum dots are also far more expensive than their colloidal counterparts, and manufacture by molecular beam epitaxy (MBE) specifically can become exceedingly expensive, especially for commercial applications²⁰.

Blinking

In colloidal quantum dots one of the main sources of discontent in the literature is photoluminescence intermittency, also known as blinking. Blinking can occur for many reasons with big contributors being non-radiative auger recombination of excitons and exciton interception before thermalisation²¹. These phenomena cause large fluctuations in the anti-bunching property of quantum dots and as a result colloidal quantum dots have reliability issues in applications like single photon emission and detection²².

Recently some solutions to this problem are being developed. The leading method for reducing blinking is by producing colloidal quantum dots with a “core-shell” structure²³. The method outlined in the paper by C. Javaux et al describes a process by which you can completely suppress non-radiative auger recombination at low temperatures, and that the auger effect only gets reintroduced in the shell at 200 K²³.

There is also evidence that ligand groups can suppress the blinking property significantly. For example a paper by Hohng et al, shows drastically reduced blinking by using β -mercaptoethanol (BME) ligands as a buffer molecule²⁵. The effects of using this buffer against a standard buffer molecule can be seen in figure 6.

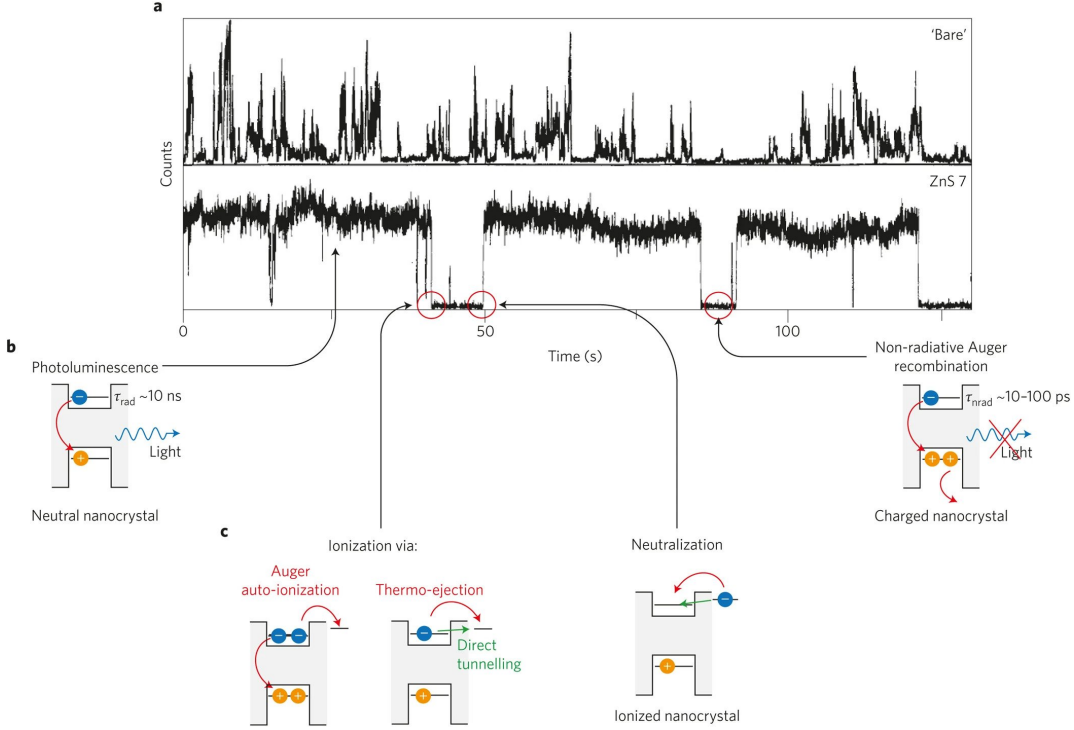


Figure 5: (a) shows presence of the Auger Effect for a CdSe cQD with no shielding in the top sub graph, and a CdSe core/ZnS shell on the bottom. We still see parts of the Auger Effect with shielding, but this can be further mitigated with different layers of shells of different semiconductor materials. (b) shows the some of the effects that may cause an E field to occur, causing the 'off' cycle of the blinking phase. We then see neutralization leading to the start of the 'on' phase of the blinking cycle and emission of light in that instant.²⁴

Single Photon Measurement and Anti-bunching

We need to first establish what a single-photon source is. To set the definition in context, imagine a setup that splits an incoming electromagnetic field into two components using a non-polarizing beamsplitter such that a time delay is introduced to one of them, and both components are individually photo-detected. Such a setup is known as a Hanbury-Brown Twiss interferometer²⁶. The degree of coherence is the normalised correlation of the two electric fields; the second degree of coherence function $g(2)$ characterises statistical nature of the intensity fluctuations of the fields and is given by²⁸ :

$$g^{(2)}(\vec{r}_1, \vec{r}_2, t_2 - t_1) = \frac{\langle \hat{n}(\vec{r}_1, t_1) \hat{n}(\vec{r}_2, t_2) \rangle}{\langle \hat{n}(\vec{r}_1, t_2) \rangle \langle \hat{n}(\vec{r}_2, t_2) \rangle} \quad (4)$$

Where \hat{n} denotes the product of the ladder operator $\hat{a}\hat{a}^\dagger$ and $\vec{r}_1, \vec{r}_2, t_1$ and t_2 denote the space-time points of the detection of the electric field. In the classical case of electric fields, this function can be expressed in terms of intensities:

$$g^{(2)}(\tau) = \frac{\langle I(t)I(t + \tau) \rangle}{\langle (I(t))^2 \rangle} \quad (5)$$

Where $I(t)$ is the intensity at time t and τ is $t_2 - t_1$. Using the second degree of coherence function, we can now quantitatively characterise a photon source. A fully coherent source of light is achieved when $g^{(2)} = 1$. This is light of a single frequency, and therefore we say that

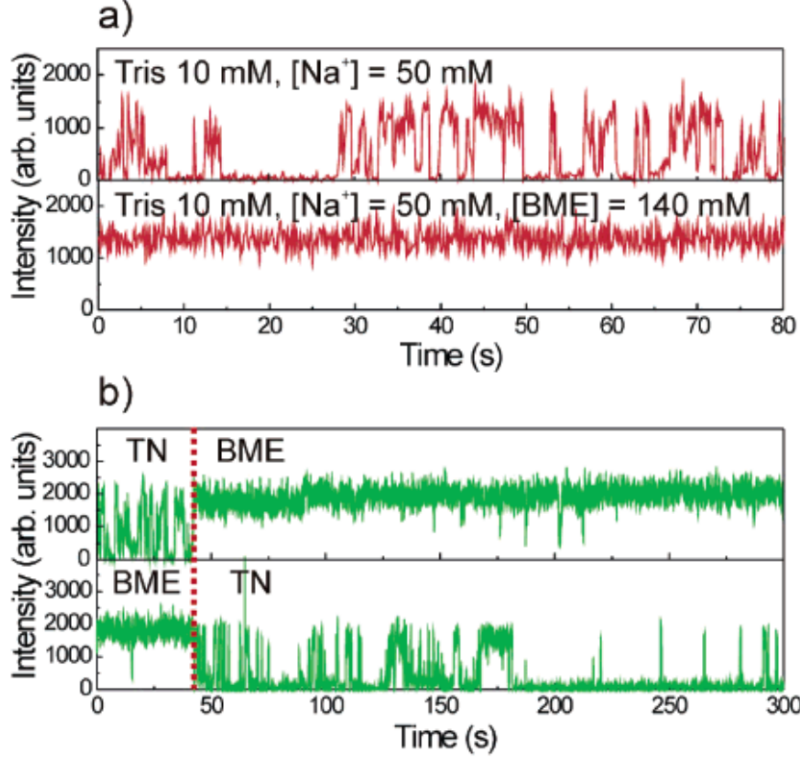


Figure 6: a upper) A typical trace from a source of CdSe quantum dots in a TN buffer solution. a lower) A corresponding trace when BME ligands are introduced as a buffer. b upper) A trace from a source of CdSe quantum dots in a TN buffer. At 40 seconds the BME ligands are introduced. b lower) A trace from a source with BME ligands as a buffer. At 40 seconds the buffer is washed away by a TN buffer²⁵.

lasers are coherent sources of light. However, they are not single-photon sources. Even if the power of the laser is reduced significantly, the output light would still be emitted as a bunch of photons. Thus, to achieve a single photon source, the photons need to be ‘anti-bunched’, and this is characterised when $g^{(2)}(0) = 0$. In other words, the probability of 2 photons being detected with no time delay is 0, and after emission of a single photon, the emitter (the QD) must be excited again to emit a second photon. In terms of practicality, the time response of the photon detectors will determine the minimum $g^{(2)}$ that can be measured even with an ideal single-photon source¹⁴.

To produce antibunching, the QD structure must be sufficiently confined; the Bohr radius of the exciton must be greater than the QD radius to produce a binding energy for the exciton given by equation 6.

$$E_B = \frac{R_E Z^2}{n^2} = \frac{\mu}{m_e} \frac{R_E}{\epsilon_r^2} \quad (6)$$

Indistinguishability is another important property to define, as it is a measure of similarities between individual photons produced from the same source. Two photons are indistinguishable if their density matrices are equal, as shown in equation 7, for a full derivation see¹³.

$$\mathcal{J}(\hat{\rho}_1, \hat{\rho}_2) = |\psi_1 \psi_2|^2 \quad (7)$$

A high indistinguishability is the corner-stone of consistent quantum technology. Producing

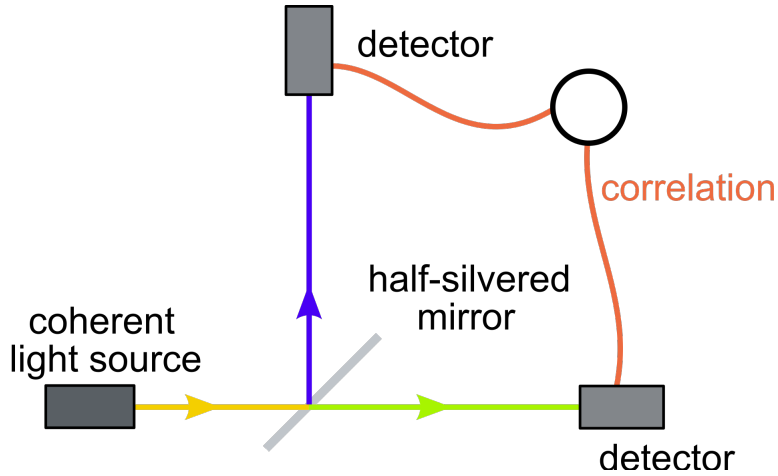


Figure 7: A schematic of the Hanbury-Brown and Twiss interferometer. The half-silvered mirror here represents the non-polarising beamsplitter. Image adapted from Wikipedia²⁷.

indistinguishable photons means that the two photon wavefunctions can interfere with one another clearly and detectors can be calibrated to detect specific properties such as spin, or polarisation as shown in equation 8 (where H is horizontally polarised photons and V is vertically polarised photons)²⁹.

$$\psi^- = \frac{1}{\sqrt{2}}(H_1V_2 - V_1H_2) \quad (8)$$

Indistinguishable photons also allow for fine control of the output mode of photons when travelling through optical devices, this can be useful in linear optical quantum computing (LOQC)³⁰. Alternatively these photons are also useful for other applications such as consistently producing identical photon pairs via spontaneous parametric down conversion (SPDC). SPDC is often the method used to produce entangled photons for use in quantum cryptography, and this indistinguishability is key to the calibration of all optical components used in quantum cryptography and quantum information applications as a whole²⁰.

Optics

Lenses

Not only is it vitally important to understand the underlying physics for the structures we are studying in the report, but it is also valuable to deeply understand the methods by which imaging is possible. Most importantly is the thin lens equation given by:

$$\frac{1}{f} = \frac{1}{o} + \frac{1}{i} \quad (9)$$

where f is the focal length of the lens, o is the distance to the object and i is the distance to the image. This equation is visualised in figure 8. Equally as important is the effective focal length equation, which is used as a mathematical tool to combine a system of multiple lenses into a single imaginary lens with a focal length equivalent to the lens system as a whole:

$$\frac{1}{f_{eff}} = \frac{1}{f_1} + \frac{1}{f_2} - \frac{d}{f_1 f_2} \quad (10)$$

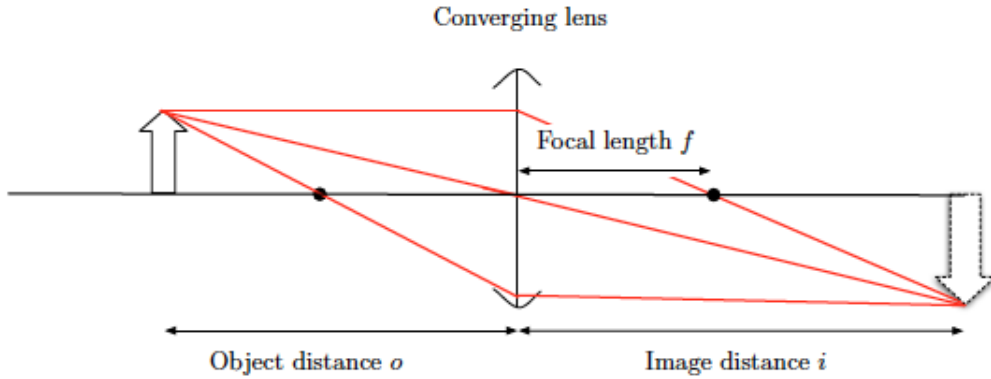


Figure 8: A typical ray diagram for a convergent lens³¹.

Where f_1 is the focal length of the first lens, f_2 is the focal length of the second lens and d is the distance between the two lenses.

When using a system of multiple lenses we will also need to consider the magnification of the image. This is given as a ratio of the focal lengths of the lenses in the system:

$$M = \frac{f_2}{f_1} \quad (11)$$

Where M is the magnification of the lens system. Using this equation is vitally important, as using a lens system with a large magnification will introduce loss of image quality due to interference associated with reaching the limit of optical microscopy; the diffraction barrier³².

Waveguides

An alternate approach to integrating QDs, which is what we will focus on in our report, is the integration of QDs into waveguides. A waveguide, as the name suggests, is a structure that guides waves with minimal loss of energy by ensuring that the transmission of energy only occurs in one direction. An experimental study done by Lodahl et al.³³ in 2008 showed that using photonic crystal waveguides (PCWs) over photonic crystal nanocavities increased quantum efficiency. This meant that the single photons emitted from the QD were transferred directly into the waveguide mode that propagated the photons. The enhanced coupling between the QD and the waveguide allowed the efficient channelling of single photons to the detector. The advantage of using waveguides is the myriad of architectures that it can provide to realise different applications. A 2013 article by Skolnick et al.³⁴ showed that by using 2 orthogonal waveguides one could configure a setup to optically control the emission direction of the single photon. Approximately 90 nm away from the centre of intersection of the waveguides, a single InAs/GaAs QD was located. Due to its location, the inversion symmetry was broken and by using the high polarizability of the exciton using optical pumping, the direction of the emitted photon was controlled. As mentioned earlier, there is a variety of waveguide architectures to be explored. The project will aim to integrate quantum dots into an optical chip that was created using lithography, however we also explore the properties of a lensed fibre waveguide.

Electromagnetic Waves

Electromagnetic waves propagate via oscillating electric and magnetic fields, those oscillations tend to occur perpendicular to the direction of propagation. However, within waveguides there can be different transverse modes that occur. This happens as a result of the dimensions and shape of the waveguide³⁵. Also as a consequence of the geometry of the waveguide there is always a lower threshold for frequency known as the cut-off frequency. Waves with a lower frequency than this can no longer propagate through the waveguide, making coupling impossible. Sometimes this can be advantageous, like using a waveguide as a high frequency pass filter³⁶. There are three different types of transverse modes, however only two can be produced within a waveguide. Starting with the two that can be produced in a waveguide: Transverse electric modes are those which have no component of the electric field oscillating in the direction of propagation, but it has some non-zero amount of magnetic field oscillating in the direction of propagation. Conversely, transverse magnetic modes are the opposite, where no component of the magnetic field is oscillating in the direction of propagation, but a non-zero component of the electric field is oscillating in the direction of propagation. Lastly Transverse Electromagnetic waves are conventional optical waves with neither electric or magnetic fields oscillating in the direction of propagation. These cannot occur in waveguides because they are single conductor systems³⁷. For the TEM mode to propagate there must be one conductor producing the voltage needed for the electric mode and a different conductor producing the currents required for the magnetic mode. In a single conductor system this is impossible to achieve as the two effects cancel each other out³⁷. There are also hybrid modes which exist where some component of both the electric and magnetic field are oscillating in the direction of propagation, however these are less relevant for our purposes as the waveguide we are working with only supports well defined modes of transport through the waveguide.

CHAPTER 3: METHODOLOGY AND RESULTS

Imaging

Investigations of the atom-photon chip and the quantum dot solutions had to be conducted qualitatively. Thus, the primary task of the project was to construct an imaging system to view them. This was achieved on an optical bench.

An initial approach to imaging was first conducted using a USB microscope, and its imaging capabilities were tested on the atom-photon chip. Preliminary USB microscope images of the chip are shown in Figure 9.



Figure 9: Preliminary USB microscope image of the atom-photon chip.

The downside to using the USB microscope was that it could not resolve the individual waveguides on the atom-photon chip which were 2 microns thick - as seen in Figure 9.

The USB microscope was replaced with a Thorlabs CCD camera. This was a DCC1545M model camera with a pixel size of 5.20 microns. Therefore, with sufficient magnification, the waveguides could be imaged. The main challenge with utilising the CCD camera for imaging was that it was monochrome in contrast to the USB microscope. Secondly, the camera did not have lenses to focus light onto its CMOS sensor. Thus, a two-lens imaging system had to be built for the camera.

Obtaining the imaging resolution using a CCD

Before imaging the atom-photon chip, the imaging system was built and tested on a USAF Positive 1951 Test Target manufactured by Thorlabs. This was to determine the maximum resolution that could be achieved using the system. Figure 10 shows the test target:

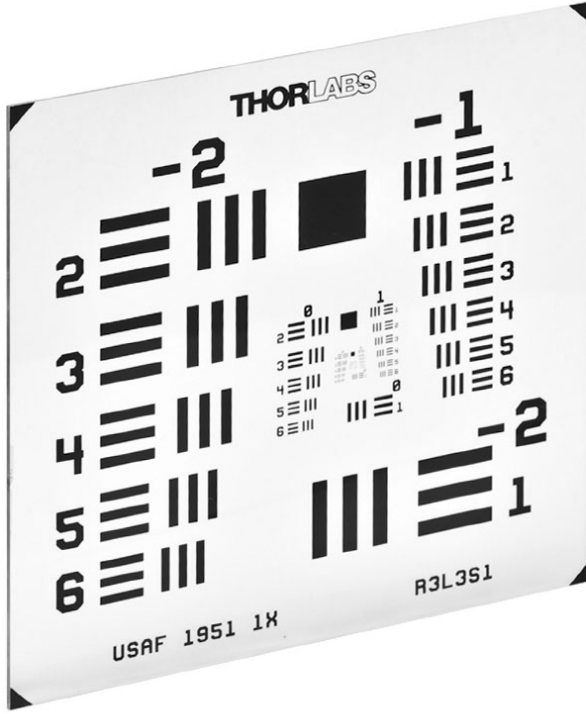


Figure 10: The 3" x 3" Thorlabs positive 1951 USAF Test Target. Product details and resolution charts are found here³⁸

The test target has 9 groups of lines going from -2 to 7, with each group containing a line set of three. The larger the group number, the smaller the lines are in the set. The resolution of an imaging system is determined by the largest set of non-distinguishable that can be viewed. The group and element number of the line set is then looked up on a Thorlabs chart³⁸ to obtain a numerical value for the resolution. The unit of resolution as per the manufacturer is given in line pair per millimetre (lp/mm), which is then doubled and then reciprocated to obtain the resolution of the system in units of length. The final image obtained with our setup (shown in Figure 11) after fine adjustments yielded a resolution of 144 lp/mm.

To obtain a resolution, R , in units of length, we do the following:

$$R = \frac{1}{2 \times 144 \text{lp/mm}} \approx 3.47 \mu\text{m} \quad (12)$$

This value is slightly larger than the 2 micron length, however, it was deemed a sufficient resolution provided the waveguides could be contrasted sufficiently. The method of creating this contrast and imaging the chip is discussed in the next section.

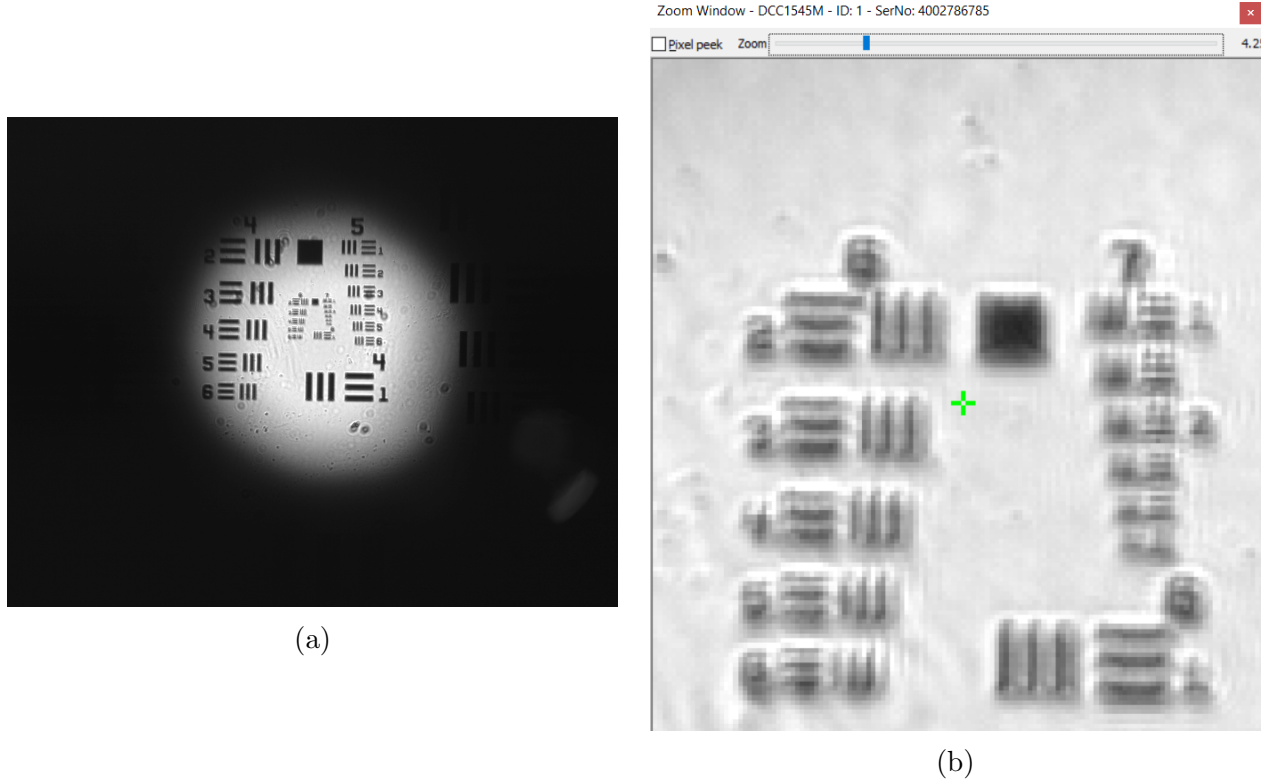


Figure 11: (a) CCD image of the test target. A pinhole was placed in front of the plate to improve image quality. (b) The zoom window of our camera viewer showing groups 6 and 7. We can clearly see that Group 7, Section 2's lines are distinguishable, which correspond to a resolution of 144 lp/mm.

Imaging the atom-photon chip

The chip was glued onto a steel post, and then was attached to a 3-axis translation stage to allow for fine adjustments. The distances between the eyepiece and the objective changed from the previous setup to obtain the optimal image. The optical setup for imaging the chip is shown Figure 12:

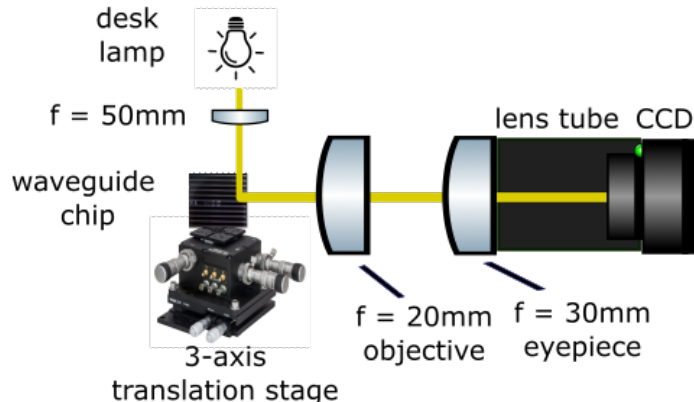


Figure 12: The optical setup for imaging the atom-photon chip. The setup is based on the multiple lens system outlined in the theory section.

To obtain a contrast on the image, a desk lamp was placed above the waveguide and light from the lamp was focused using a 50mm focal length convex lens onto the edge of the chip facing the waveguide. This allowed for a sharper image with fewer stray reflections from the chip. Figure 13 shows the CCD image captured using our setup. We see that there is sufficient magnification and contrast to see the repeating pair of bright spots which are the gaps between the waveguides.

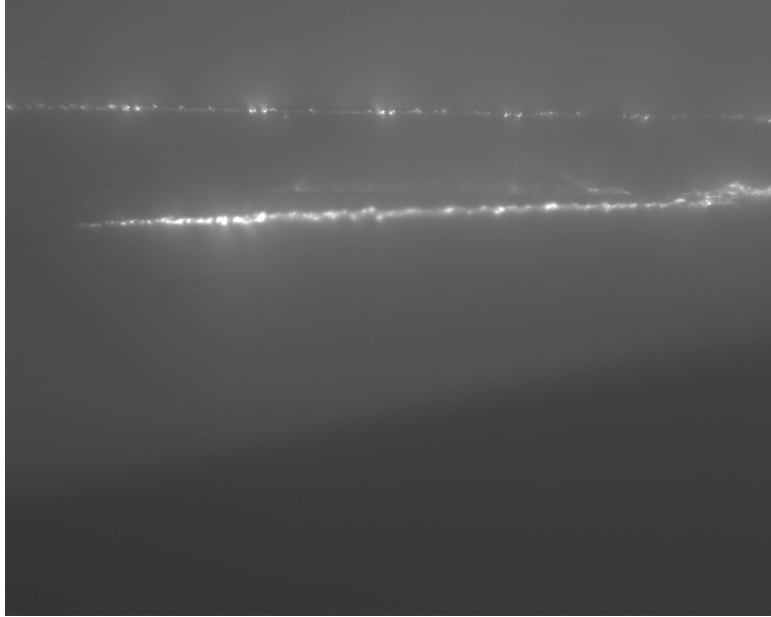


Figure 13: CCD image of the atom-photon chip showing the waveguides. The repeating pair of bright spots are the gaps between the waveguides.

Preparing the samples

The quantum dots used for imaging were CdSeS/ZnS alloyed dots from Sigma Aldrich. They had an emission wavelength of 665nm with a 6nm diameter stored with a concentration of 1 mg/mL in toluene. Based on literature outlining the preparation of quantum dot samples onto microscope slides, a concentration of 10^{-9} - 10^{-11} MOL was optimal for imaging. The first step was to obtain an approximate concentration in units of molars based on the dimensions of the quantum dot and the solution. We need to calculate the mass of a single quantum dot, m , using the density of quantum dots, ρ and its volume, V :

$$m = \rho V \quad (13)$$

There are 1000 grams of quantum dots per metre cubed. The volume of a single dot can be calculated from its radius, $R = 3\text{nm}$, assuming it is spherical:

$$V = \frac{4}{3}\pi R^3 = \frac{4}{3}\pi(3 \times 10^{-9})^3 = 1.13 \times 10^{-25} m^3 \quad (14)$$

Using this approximation, the mass of a quantum dot is

$$m = 1000 g/m^3 \times 1.13 \times 10^{-25} m^3 = 1.13 \times 10^{-22} g/qdot \quad (15)$$

METHODOLOGY AND RESULTS

We first diluted the solution to 10^{-5} MOL by taking 0.01 mL of CdSeS/ZnS solution and dissolving it in 9.99 mL of toluene. There are 0.01 mg of quantum dots in 0.01 mL of solution, so the number of quantum dots in 0.01 mL is:

$$\frac{1 \times 10^{-5}g}{1.13 \times 10^{-22}g/qdot} = 8.85 \times 10^{16} qdots \quad (16)$$

The number of moles of quantum dots, n , can be calculated using Avogadro's constant:

$$n = \frac{8.85 \times 10^{16}}{N_A} = 1.47 \times 10^{-7} moles \quad (17)$$

Thus, after the first dilution, the molar concentration, M , is given by:

$$M = \frac{n}{V_s} = \frac{1.47 \times 10^{-7}}{10 \times 10^{-3}} = 1.47 \times 10^{-5} MOL \quad (18)$$

V_s is the volume of the total diluted solution, which is $0.01\text{mL} + 9.99\text{mL} = 10.00\text{mL}$.

This procedure was done 3 more times using 0.1 mL of the diluted solutions obtained after each repeat to get concentrations of 10^{-7} , 10^{-9} and 10^{-11} MOL.

After preparing the samples, we altered our optical setup for imaging the quantum dots. We introduced a 532nm green laser to excite the quantum dots. The laser light was reflected off two mirrors on mirror mounts. These mirrors were used to fine adjust the position of the laser light. A 605 nm cut-off wavelength dichroic mirror was placed in the imaging system to only transmit the emission from the dots. The schematic of the setup is shown below:

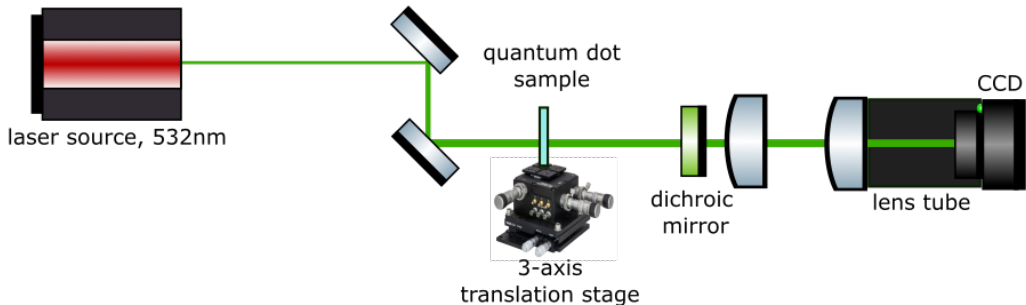


Figure 14: The optical setup for imaging the quantum dot sample on a microscope slide. The dichroic mirror, which has a cut-off frequency of 605nm, filters the excitation wavelength (532nm) from the emission wavelength (665nm)

An initial method of preparing the slides was to drop approximately 0.1 mL of the diluted solution onto a microscope slide, and then allow the toluene to evaporate so that only the quantum dots were left on the slide. We noticed that due to surface tension the quantum dots clumped together during evaporation. After fine adjusting the laser light and the positions of the CCD and the objective lens, we obtained an image of a sample of 10^{-11} MOL quantum dots:

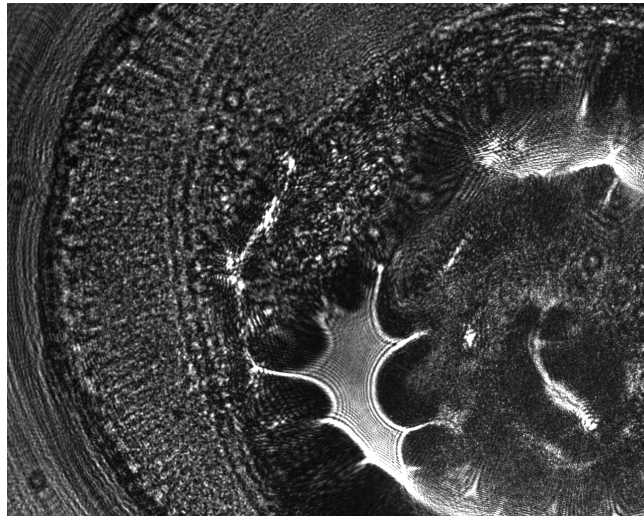


Figure 15: CCD image of a sample of 10^{-11} MOL CdSeS/ZnS quantum dots after allowing the toluene to evaporate.

Spin Coating and microscope objective imaging

The CCD image, Figure 15, has a lot of diffraction effects going on and needed to be magnified further to evaluate if the plethora of bright spots are indeed quantum dots. Thus, the dots needed to be distributed evenly and a higher magnification imaging system was required to image individual dots. To achieve an even density of dots, microscope slides were spin coated with the quantum dot solutions. There were two spin coating methods done for this project. The first was to spin coat the slides at 200 rpm for 60 seconds and allow the toluene to evaporate during that time, so that only the quantum dots remained. The second was to spin coat another set of slides at 500 rpm for 15 seconds and then place a coverslip on top of the slide to hold the toluene and quantum dots solution in place. The coverslip was attached to the slide by super-gluing it on the corners.

The reason for doing these two spin coating mechanisms was to see if the presence of toluene affected the image quality. To achieve a higher magnification imaging system, we used a 20x, 0.4 numerical aperture microscope objective lens. This was our final optical setup for imaging the quantum dots:

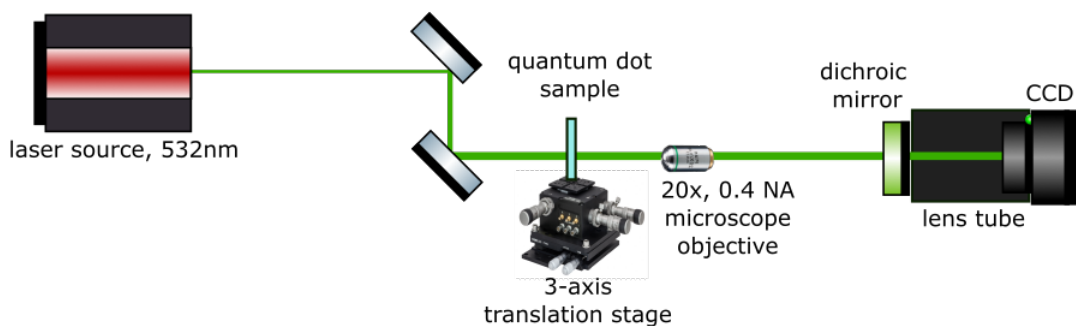


Figure 16: Improved optical setup to image the quantum dot sample using a 20x microscope.

Below (Figure 17 is an image of the 10^{-11} MOL sample without a coverslip:

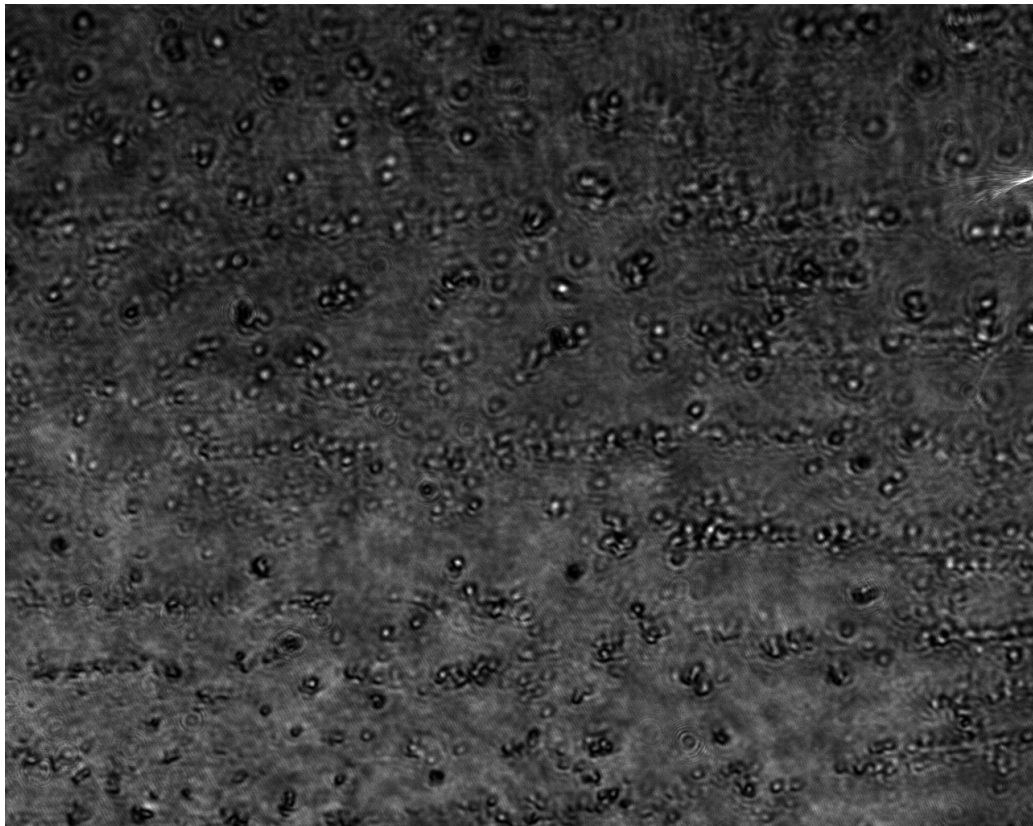


Figure 17: CCD image of a sample of 10^{-11} MOL CdSeS/Zns quantum dots taken after spin coating and allowing the toluene to evaporate. Taken using a 20x microscope objective.

The Thorlabs camera software allows you to change the exposure time of the camera and to change the gamma value of the imaging. The human eye perceives differences in the brightness of a scene based on a logarithmic characteristic, and this perception is approximated using a gamma characteristic in imaging. For computers, a gamma value of 2.2 is used, and is the same value used for this project. Exposure time is the length of time light is collected by the camera.

To further distinguish the background light from the emission of the quantum dots, the exposure time was lowered, which meant that less light entered the camera. In turn this would only allow the emission from the quantum dots to be seen and would prevent majority of the background light and light reflecting off any potential dust particles to enter the camera. To achieve the lowest exposure time with visible quantum dots on the image, the gamma was set to 2.2. Figure 18 shows the same image of the 10^{-11} MOL sample without a coverslip shown previously, but with an exposure time of 0.857 s.

With a very low exposure time, we see that there are only a few bright spots left, which we conclude are the quantum dots. The Thorlabs imaging software enable us to choose areas of interest (shown in blue and red in Figure 18). The selected areas are shown in Figure 19. We took a 3 minute video of the blue area of interest (found in the supplementary material under `aoi-3min.avi`) to observe if there was any blinking. The pixel values did change, but this was only due to the noise of the camera, caused mainly by the high gain required for a low exposure time. Therefore, we didn't notice any blinking, and we go into potential reasons

as to why this was the case in section 4.

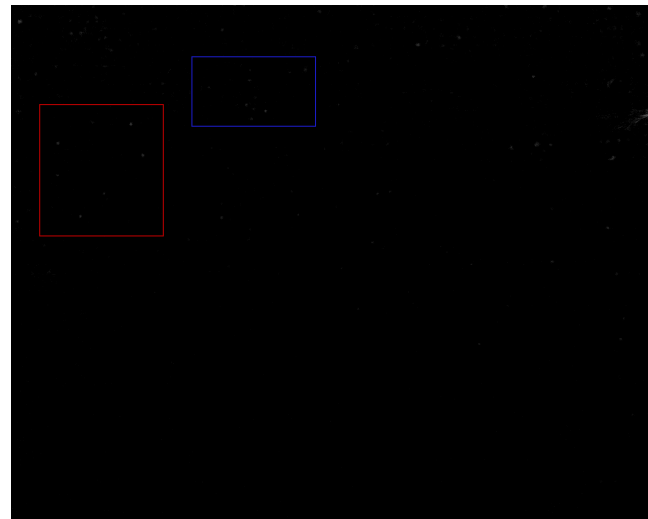
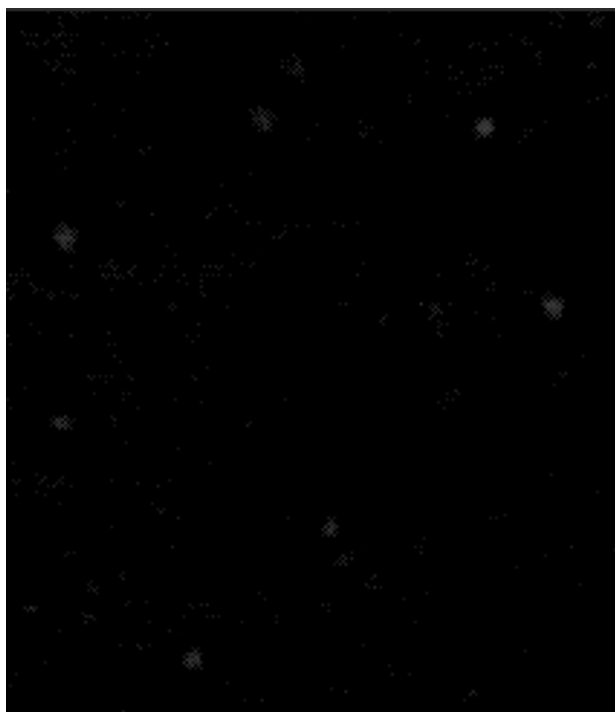


Figure 18: CCD image of a sample of 10^{-11} MOL CdSeS/Zns quantum dots taken after spin coating and allowing the toluene to evaporate. Taken using a 20x microscope objective with an exposure time of 0.857s. The blue and red areas are areas of interest that can be studied further.



(a)



(b)

Figure 19: (a) Red area of interest. (b) Blue area of interest. A 3 minute long video of this area of interest can be found in the supplementary material under the file name `aoi-3min.avi`

With regards to the sample that had a cover slip on top, the high exposure and low exposure images are shown in Figure 20. From comparison, we can see that the bright spots are more visible and clear when there is no cover slip on top, but there is a higher possibility of dust accumulating on the surface in that scenario.

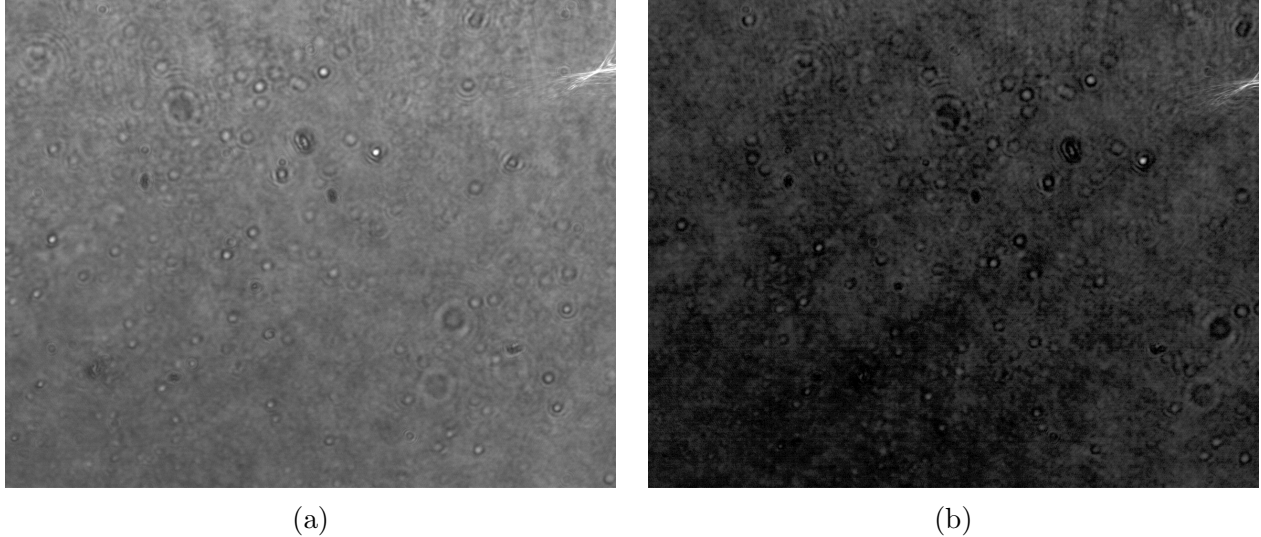


Figure 20: (a) High exposure and (b) low exposure images of the 10^{-11} MOL CdSeS/Zns quantum dots taken with a cover slip on the slide.

Coupling Mechanisms

Using an aspherical lens

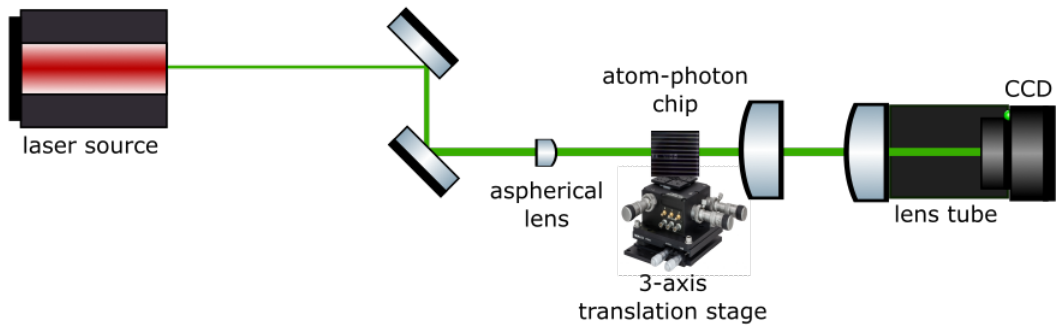


Figure 21: The experimental setup of the key optical components involved in the aspherical lens coupling mechanism.

Our first attempt at coupling to the waveguide chip was made using the setup shown in figure 21. We used a two mirror setup would allow fine control over the position of the laser light. To do this the mirrors were mounted on rotation stages, which allowed each mirror to be rotated in the orthogonal and azimuthal planes. The aspherical lens was positioned such that incoming laser light would converge in the same plane as the waveguide chip.

The concept for this method is that adjustments to the position of the laser would be the main method of coarse position adjustments, and that the 3d translation stage could handle the fine adjustments to tweak the position of the waveguide for better coupling. We used the CCD imaging setup as our only guide for positioning the waveguide. We had previously illuminated the waveguide with a torch light from above, and so when checking the CCD using the laser, we checked for similarities, as we anticipated that coupling would look as though a waveguide track has been illuminated in a similar way.

Our results while measuring using this method show a clear contrast between the waveguide chip and the incoming laser light, but it is certain that coupling never occurred strongly enough to visualise any outgoing light with the use of the digital microscope. Our imaging setup produced the pattern shown in figure 22

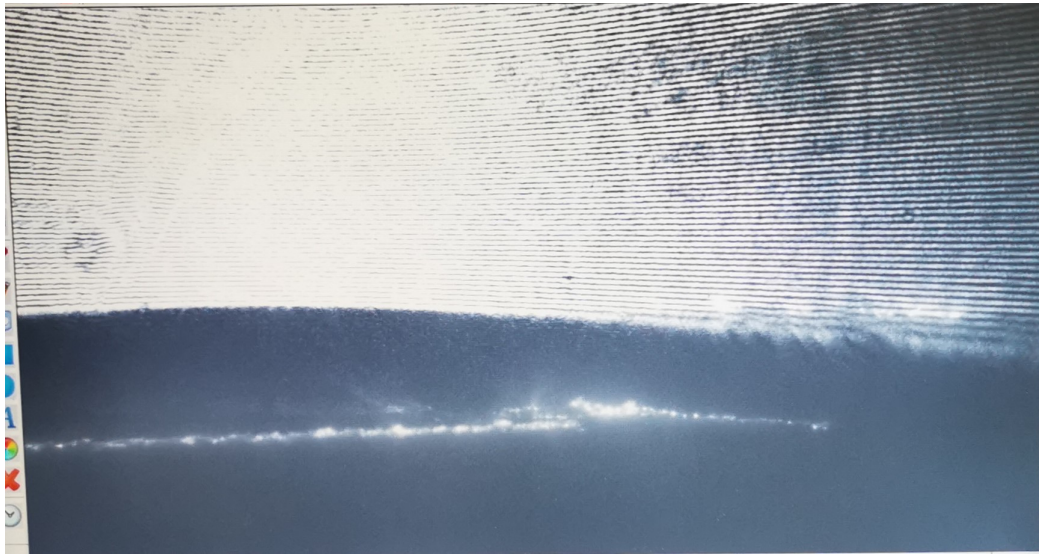


Figure 22: An image taken from the CCD sensor, focused on the front of the waveguide chip when laser light from an aspherical lens is shone into the waveguide.

Lensed Fibre & Butt-Coupler

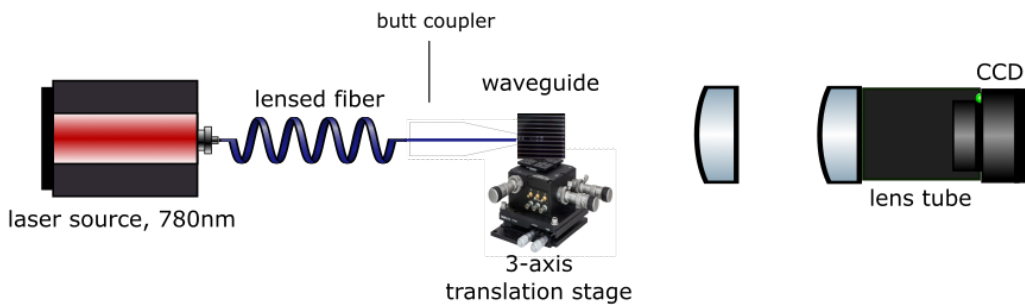


Figure 23: A diagram showing the positions of the key optical components used for the lensed fibre coupling mechanism.

We stopped our progress with the aspherical lens setup, due to a combination of the unstable positioning of the laser light and difficulty getting the laser beam to a small enough radius to

couple effectively into the waveguide; we moved onto other methods of coupling.

We changed the mirror setup shown in figure 21 for the setup shown in figure 23. The lensed fibre has a working distance of $10\text{ }\mu\text{m}$, which means the fibre must be placed right against the waveguide. This feature makes it possible for very fine translations and rotations of the waveguide, while maintaining the position of the focal plane of the laser light.

As a consequence of using this fibre, we also invested in a butt-coupler. A device which can be clamped directly next to the waveguide which is used to hold the fibre in place with rubber tipped magnetic elements. The butt-coupler is required because the fibre is far more fragile than standard fibres which are protected with plastic casings, and can therefore be clamped in place with little risk of damaging the fibre within. The lensed fibre is far thinner than standard fibres and moreover cannot be fitted with a bnc connector, which work to keep standard fibres in place.

The method we used when attempting to couple light into the waveguide was simple. Instead of walking the laser beam position (as with the aspherical lens setup) instead we would walk the position of the waveguide chip using the translation stage. For this particular method we also mounted the waveguide chip to a mirror rotation stage which gave us far more control over the orthogonal and azimuthal degrees of freedom (shown in figure 24). Something particular to note is that when rotating the azimuthal component, we would have to recenter the waveguide by readjusting the x component afterwards. Similarly, when rotating the orthogonal component, it would always require readjusting the z component afterwards. These adjustments were made to keep the waveguide in line with the lensed fibre because we found that although the rotation components mainly corresponded to rotational movement, there was also a small amount of translation that needed to be offset, as described.



Figure 24: An image of the newly added mirror mount. This component expands our fine adjustments of the waveguide chip from three degrees of freedom, to five degrees of freedom.

Another improvement we made to the method while testing the lensed fibre was to add another two cameras. The digital microscope to image a top down perspective of the waveguide (shown in figure 25) and another high resolution digital camera to image a side view of the waveguide and the butt coupler. These cameras could take images between each small adjustment and

worked well to show if we were coming closer to achieving coupling with each subsequent movement.

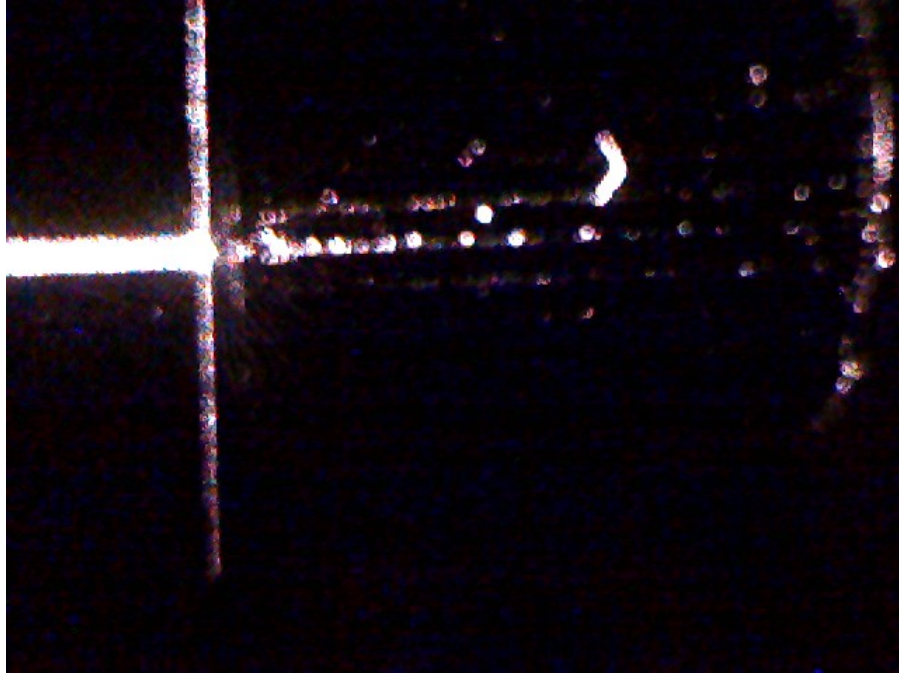


Figure 25: An image taken from the digital microscope setup. It was positioned directly above the waveguide setup and proved extremely useful for aligning the x , θ and ϕ degrees of freedom with the butt-coupler.

Using this method of coupling, we were able to achieve a coupling efficiency of 61% between the laser source and the end of the lensed fibre. We were also able to achieve some visual signs of coupling as shown in figure 26. Unfortunately, due to the position of the waveguide needing to be precise down to the micro scale, as we were attempting to measure the transmittance through the waveguide element, the coupling was lost due to accidental adjustments to the position of the waveguide relative to the fibre and we were never able to realign the positions in order to regain efficient coupling.

The images shown in figure 26 provide good evidence for coupling having been achieved through the waveguide. We also imaged this coupling from the front facing CCD setup shown in figure 27. However the results were hard to distinguish and similar to figure 22 as a consequence of too much stray laser light incoming from over the top and around the edges of the waveguide chip. This results in very clear diffraction patterns from the reflections of stray light against the waveguide chip.

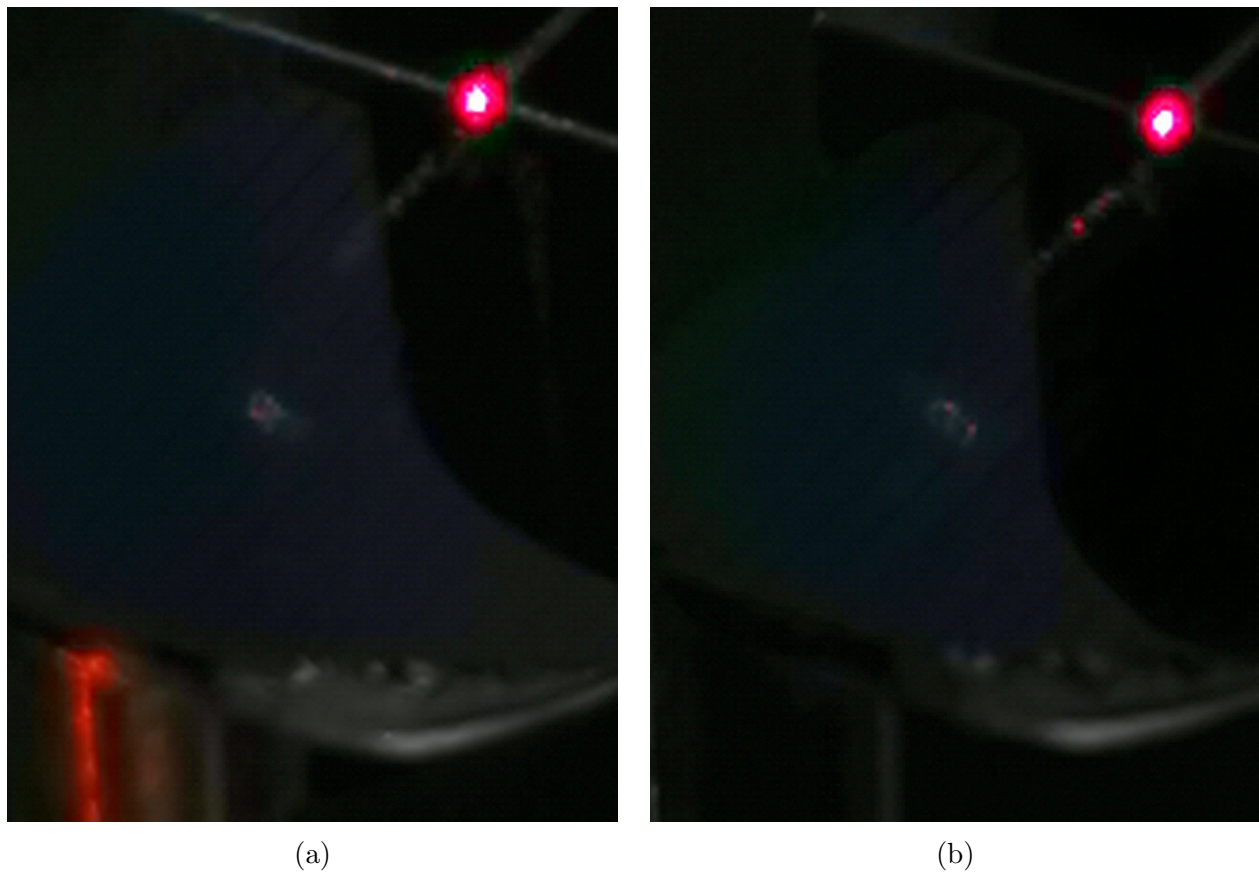


Figure 26: a) Visual signs of coupling via outgoing red beam on the close side of the waveguide.
b) No signs of coupling as the close side of the waveguide chip remains dark.



Figure 27: An image taken with the CCD setup which is focused on the front of the waveguide chip.

CHAPTER 4: DISCUSSION

Review of Imaging System

At the beginning of the project, we attempted to image the test target with an eyepiece convex lens of a focal length of 50mm; this was the image that was obtained:

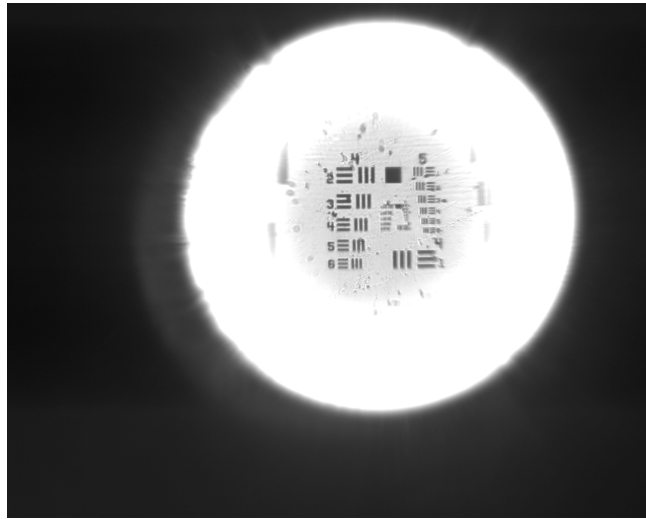


Figure 28: CCD image of test target using a 50mm focal length eyepiece

Theoretically, using a higher focal length convex lens produces a more magnified image than using a lower focal length lens. So, we now know that we could have obtained a better image than the one shown above with the 50mm lens. Working on an optics bench was unfamiliar territory for us at the beginning of the project, however in the future it would be better to experiment with an imaging system with lenses that have a higher focal length.

In addition to higher magnification, another advantage to using higher focal length lenses is that the CCD camera would be much further away from the atom photon chip. A longer distance between the camera and the chip would possibly yield an imaging system that could distinguish between light hitting the back of the chip and light that passes through the waveguides, as light reflecting off the back of the chip would have a lower intensity compared to light transmitted. Optically, this would be a more convenient method off confirming whether the waveguides were coupled or not to the laser light.

Another characteristic we noticed in the image obtained using the 50mm lens is that the edges of the image looked warped. We later realised that this was most likely spherical aberrations, which may have been caused due to the convex nature of the lens. The 50 mm lens was a biconvex lens, conversely the lenses we used in our final imaging system of the waveguide were plano-convex lenses. A plano-convex lens used as an eyepiece can reduce spherical aberrations to a minimum when the convex surface faces the object being imaged. This may have been why it was easier for us to image with the shorter focal length lenses

because they were both plano-convex.

Along with using higher focal length lenses, an additional optical component to integrate and experiment with in the future would be an aspherical lens. Aspherical lenses focus uncollimated beams, however, light that emerges from a point source are collimated by aspherical lenses. If we consider the coupled light from a waveguide to be light emerging from a point source, then an aspherical lens could further distinguish between light arising from coupling and light reflected off the back off the chip. This is because the coupled light would be collimated and would render as a higher intensity reading on the camera, while any other stray reflections or diffractions would have a lower intensity.

A more stable approach to imaging the waveguide is using an infinity corrected microscope objective in conjunction with a convex lens as an eyepiece. In an infinity connected system, the light beam that passes through the objective does not form an image but forms an infinity parallel beam which can then be focused down to an image using an eyepiece. The advantage of this system over using just using convex lenses is that you can maintain the high magnification at longer distances. Thus, we can control and minimise the intensity of stray reflections compared to coupled light more efficiently with this system. Future work may try to integrate an infinity corrected microscope for imaging to achieve more distinguishable coupling patterns.

Review of Blinking Observations in Quantum Dots

We are confident that the images obtained of the quantum dot samples are indeed quantum dots and not dust particles. To confirm this, we took an image of a microscope slide that just had toluene on it, and an image of a plain microscope slide:

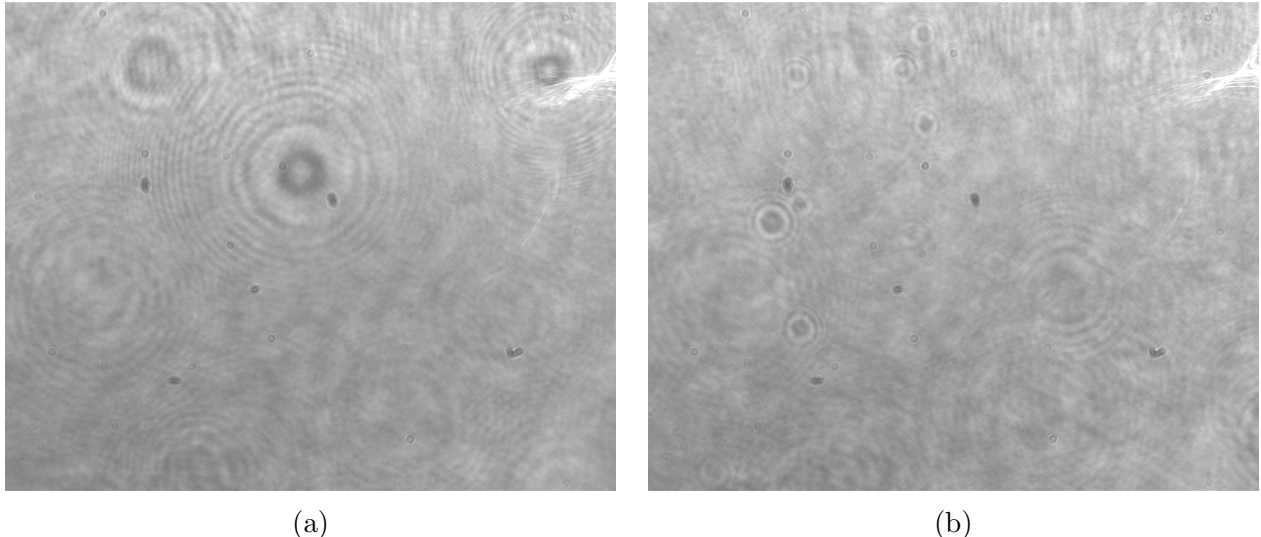


Figure 29: (a) CCD image of a toluene sample, (b) CCD image of a plain microscope slide

We see that there are fewer bright spots on both those images, and after lowering the exposure time to 0.857 s (this value was used to image the dot samples), the spots weren't visible at all.

This meant that the slides that contained quantum dot samples could potentially have

dust particles too. A better job could have been done in preparing the slides. For our preparation, we cleaned the slides using a lens tissue cleaner and propanol. However, in the paper by Frazer et. al.³⁹ that was mentioned earlier outlining the preparation of quantum dot samples for imaging, the slides were stored in distilled water until the samples were spin coated on them. This method would have ensured fewer dust particles on the surface of the slide, and hence a cleaner imaging sample. A more important critique to note is the potential lack of magnification that our imaging system possessed. While the 20x objective provided relatively good images compared to the dual lens imaging system, Frazer et. al.³⁹ used a 100x objective to image the dots, and subsequently noticed blinking in their research.

This led us to conclude that while we did see quantum dots, what was imaged was in fact clusters of quantum dots instead of individual quantum dots. We were unable to obtain a 100x objective; we predict that if the imaging system utilised this objective, we would be able to notice blinking. It is difficult to notice any blinking with a lower magnification since different quantum dots in the same sample could have a variety of blinking times, and what you notice as an output is one continuous bright spot produced by a cluster of dots. If this project were to be conducted in the future, a comparison of the images produced by a 20X objective and 100X objective must be achieved.

Another theory as to why we did not notice blinking could have arisen from the nature of the quantum dot shell. In recent years, relatively thick CdS shells have been synthesised on quantum dot cores such as CdSe to suppress blinking^{40 41}. Work done by Qin et. al.⁴² demonstrated that the synthesis of ZnS shells around CdSeS dots (which is the sample imaged for this project) also produced photostable and bright dots. This reasoning sheds more light as to why Frazer et. al.³⁹ noticed that dots with a shell were mostly bright (with an approximate duration of 10 seconds of darkness) for the recorded time, but dots without a shell were mostly dark.

With regards to our project, the presence of ZnS shells may not be the primary factor as to why we did not notice blinking, but in the future, imaging with a higher magnification can allow for extended work to be done on investigating dots with a shell and dots without one, and their effects on quantum information applications.

In summary our work studying the blinking effect of colloidal quantum dots produced valuable insight to the scale at which blinking maybe be visible and the possible time scale on which blinking occurs. As a product of using only alloyed quantum dots, we were able to observe stable emission from our imaging system. Though we are unsure whether the cause was due to the core shell structure providing more photostability than other species of dots such as unshielded chalcogenides, or whether the imaging system was lacking the magnification to truly isolate individual dots to observe blinking. The truth is likely a combination of both reasons.

Review of Coupling Mechanisms

As highlighted in section 3.3 We demonstrated two different potential methods for coupling a laser beam to a waveguide device. The method which yielded the best results was by using a lensed fibre and a butt-coupler. We believe there is potential for the method using aspherical lenses to work given more time. In this section we intend to highlight some improvements that

DISCUSSION

could be made to both the aspherical lens setup and the lensed fibre setup in order to improve the results for future work.

Focusing on the aspherical lens setup first, multiple aspherical lenses may improve the ability to couple into a waveguide chip significantly and could generate results consistent with the 2019 paper by Badri et al. Who performed simulations using a Maxwell Fish Eye lens⁴³. A problem that has yet to be researched as far as we can see is whether or not the beam radius makes a substantial difference to the difficulty of coupling laser light into a waveguide chip. The hypothesis we have is that using a laser beam with a radius comparable to that of the radius of the waveguide chip could help to reduce the difficulty and improve the efficiency of the coupling. This could be a reason why the lensed fibre method worked much better than the aspherical lens method, as the outgoing laser beam from the lensed fibre was significantly smaller in radius compared to the laser source from the aspherical lens setup, though more work would have to be done to quantify this assessment.

Another potential improvement that could be made to our setup was to produce a better columnated laser source before coupling into the lensed fibre or the waveguide chip. Our light source, although roughly columnated at short distances did begin to diverge slowly as the optical distance from the target was increased. This likely impacted the results produced from the aspherical lens setup drastically, as the light source reaching the waveguide would have a larger beam radius and therefore impacts the proportion of light which reflects around and above the waveguide chip rather than coupling through. This would certainly impact on the difficulty of imaging the waveguide chip as stray light plagued the CCD imaging system significantly throughout our experiments.

A set back which had considerable impact on the efficiency of the coupling for all the coupling mechanisms was the goodness of the laser source to begin with. Referring to the image in figure 30, it is clear that the 780 nm laser has major problems. The outgoing beam is supposed to be gaussian in nature, so seeing artifacts reminiscent of a double slit experiment shows the laser is not functioning correctly. This would've effected the coupling efficiency of the laser into the waveguide for the aspherical lens mechanism and also the coupling efficiency into lensed fibre for the butt-coupler mechanism.

One problem that arose during our time using the lensed fibre was the coupling of the laser source into the lensed fibre becoming decoupled. As a consequence we spent some time trying to reposition the laser light source using a combination of mirrors similar to the setup used for the aspherical lens method. To recouple the source to the fibre we measured the intensity of the light through the fibre by attaching it to a photodiode, and reading the output via an oscilloscope. While recoupling, it became clear that an ideal lensed fibre should carry 100% of light from the laser source. In other words it should be a lossless fibre. However with our fibre we could only gain an output of 61%. Perhaps the results of improving coupling at this stage would be negligible when compared to the other factors mentioned. But nonetheless it could prove to be a limiting factor for future work, given that the other issues mentioned have been eliminated.

It's important that further work be done on whether waveguide chips can accept input of a different wavelength to the output wavelength as this vital aspect of the work for integrating colloidal quantum dots into waveguide chip components. This is because for the waveguide chip to function as a single photon emission element in quantum information applications it

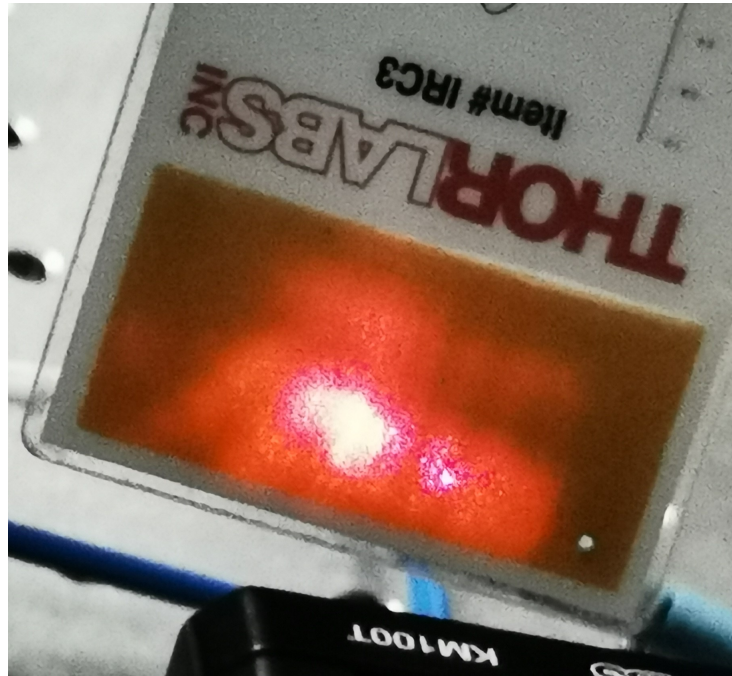


Figure 30: An image taken of the outgoing laser light against a Thorlabs beam card designed to illuminate light which would be invisible to the naked eye. Artifacts characteristic of the double slit experiment can be seen.

must accept the excitation wavelength of light which is incident as a super-poissonian source then also carry the emitted sub-poissonian source which propagates with a different wavelength.

The coupling mechanisms discussed in this report were successful in proving the possibility of transferring light from a fibre waveguide to a waveguide chip. This is highly significant for applications in quantum computing and information, as within these fields light acts as a carrier of information and therefore methods of transferring light from one component to another in an efficient manner is valuable progression towards realising scalable quantum devices.

CHAPTER 5: OUTLOOK

Testing Single Photon Emission of Quantum Dots

The motivation and the aim of this project was to test whether quantum dots on the atom-photon chip could behave as single photon emitters. In addition to this objective, we wished to investigate whether the waveguides on the chip enhanced the single photon nature of the quantum emitters.

A major roadblock in this project was possessing quantum dots with a different emission wavelength to the one the waveguide chip is designed to accept. The lensed fibre we used to couple laser light to the waveguide only transmitted light at a wavelength of 780nm (IR laser light). However, the CdSeS/ZnS dots had an emission wavelength that was lower than the transmission wavelength of the fibre (665nm). For future experimentation, ordering and using quantum dots that have a higher emission wavelength than the IR laser is required. We would suggest using lead sulphide (PbS) dots, since that species have an emission wavelength of 900 nm – 1400 nm, which most likely can guarantee quantum dot excitation.

To integrate quantum dots onto the chip, we would simply use a pipette with a needle to drop quantum dot solutions and ensure that the solutions are in the gaps between the waveguides of the atom photon chip. This can be done with the assistance of a USB camera above the chip.

In the theory section, we briefly discussed on how a Hanbury Brown-Twiss interferometer could measure the second order correlation function. We would employ such a system; a proposed schematic is shown in Figure 31:

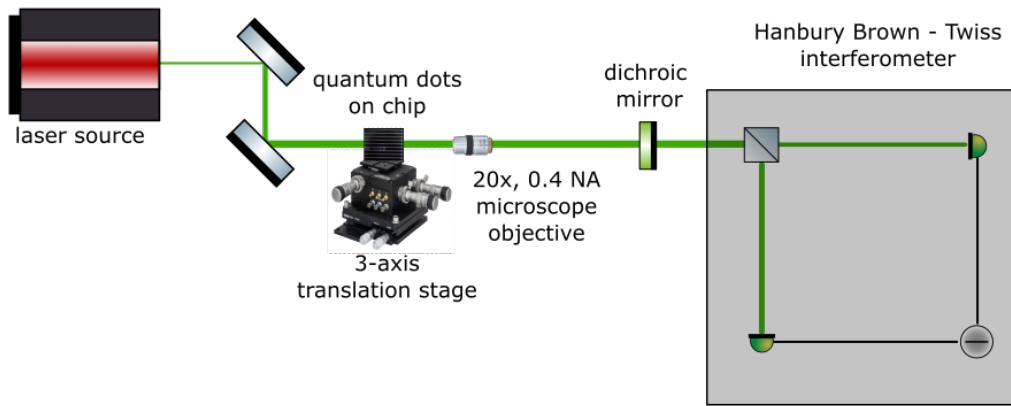


Figure 31: A proposed schematic of integrating a Hanbury Brown-Twiss interferometer to atom-photon chip setup to observe the second order correlation function.

Photodetectors on either side of the beam splitter count the incoming photons. There is a time delay, τ , between the photon counts of each detector, and this delay is then measured (shown by the negative sign in the setup). A proposed device to measure the time difference between photon counts is a time amplitude converter, which is very precise for measuring relatively

small-time differences.

Therefore, the output obtained from this experiment are not photon counts, but rather a histogram of time differences between the detection events, as shown in Figure 32:

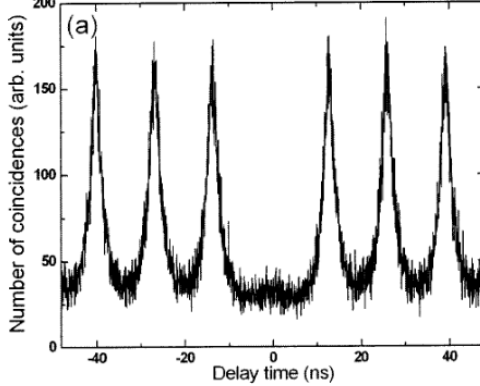


Figure 32: Histogram of time differences between the detection events obtained by work done by Zwiller et.al⁴⁴. Zwiller showed that InP quantum dots could behave as single photon sources by utilising a Hanbury Brown-Twiss interferometer to produce this characteristic distribution, which is proportional to the second order correlation function.

This distribution is proportional to the second order correlation function in the limit of a low count rate (where $\tau \ll$ average time between two detection events). If the quantum dots we use are indeed single photon sources, we will see a suppression of the $\tau = 0$ coincidence counts in our histogram. Further investigation of the effect of the waveguides (on the atom-photon chip) on the single photon nature of the quantum dots can be done comparing the histograms obtained with and without chip. If the chip enhances the single photon nature of the quantum dots, there should be a further suppression of the $\tau = 0$ coincidence counts on its histogram.

Quantum Information Applications

The overarching goal of this project is to provide methods of producing a reliable and scalable component which can act as a single photon source. This is a key part of realising commercially viable quantum information devices such as quantum repeaters and quantum key generation for quantum cryptography^{45 46}.

Although our research fell short of measuring a quantum efficiency in our apparatus, we have sufficient evidence to suggest that our methods do work, and will likely work well if quantum dots are integrated into the system. One reason for this is that the biggest benefit of our experiment is that coupling was achieved while maintaining room temperature, where no doubt lattice vibrations throughout the waveguide itself made the device far less efficient. As a result it is fair to infer that if quantum dots were integrated into the system in future research it could show promising results⁴⁷.

Previous work by Masud et al.⁴⁷ showed that when a waveguide cavity is filled with a quantum dot solution such as CdSeTe/ZnS the transmission experienced from the waveguide is enhanced significantly compared to when the cavity is empty. Although this work was done using a zero mode waveguide rather than a waveguide chip, we believe that this still shows promise that

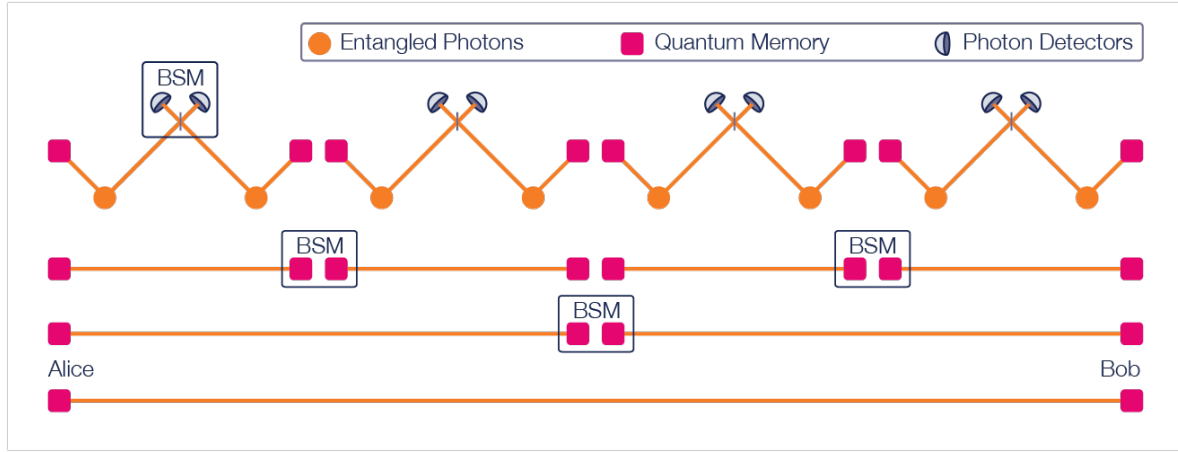


Figure 33: A schematic diagram of a potential quantum repeater. With accompanying diagrams for the classic Bob and Alice quantum key distribution system involved in quantum cryptography.⁴⁶

inserting the quantum dot solution into the waveguide could've proven to produced enhanced coupling compared to what we observed in our work.

The highest quantum efficiencies reached in 1998 were around 60% and have drastically improved over the last two decades. Now almost perfect quantum efficiencies have been achieved by III-Nitride quantum dots, perovskite quantum dots and nitrogen-vacancy center emitters at low temperatures^{48 49 50}. As a result it is no longer the limiting factor in quantum devices (at least in low temperature systems). Therefore we are glad to have shown a method of propagating coherent light through space in room temperature conditions, as it provides insight into the future of quantum computing and quantum repeater devices.⁵¹

During our work we have also shown the possibility to send light from one optical waveguide to another. This is useful as it provides one step in the direction of achieving quantum repeaters, where all that remains is to place a bell-state measurement device between the two optical waveguides as shown in figure 33.

CHAPTER 6: CONCLUSIONS

This work succeeded in building a high resolution imaging system to enable the investigation of the properties of quantum dots as an emitter and also to determine the suitability of waveguide chips as a medium to contain quantum dots and channel light emitted from them. We were able to investigate both the quantum dots and the waveguides individually, furthermore we also found promising results that the waveguide can channel light from one end to the other when the incident light is of a wavelength suitable for transmission. More work should be done to investigate the two elements of our study in combination, by placing the quantum dots into a waveguide cavity and observing if transmission is possible, or even enhanced by this process.

Overall we hope to have highlighted some viable methods of coupling light to a waveguide chip and showcased a method of imaging quantum dots. The methods shown in our report could be used in future work to complete the objectives highlighted in our discussion and outlook section.

BIBLIOGRAPHY

- [1] Atominstitut, A. T.-W. ErBeStA project. 2021; <https://www.erbesta.eu/?tag=paper>.
- [2] MacFarlane, A. G. J.; Dowling, J. P.; Milburn, G. J. Quantum technology: the second quantum revolution. *Philosophical Transactions of the Royal Society of London. Series A: Mathematical, Physical and Engineering Sciences* **2003**, *361*, 1655–1674.
- [3] Senellart, P.; Solomon, G.; White, A. High-performance semiconductor quantum-dot single-photon sources. *Nat Nanotechnol* **2017**, *12*, 1026–1039.
- [4] Shields, A. J. Semiconductor quantum light sources. *Nature Photonics* **2007**, *1*, 215–223.
- [5] Peyronel, T.; Firstenberg, O.; Liang, Q.-Y.; Hofferberth, S.; Gorshkov, A. V.; Pohl, T.; Lukin, M. D.; Vuletić, V. Quantum nonlinear optics with single photons enabled by strongly interacting atoms. *Nature* **2012**, *488*, 57–60.
- [6] Day, C. Antibunching observed in cold, dense gases of fermionic atoms. *Physics Today* **2007**, *60*, 18–20.
- [7] Ozawa, M. Heisenberg’s Original Derivation of the Uncertainty Principle and its Universally Valid Reformulations. *Current science* **2015**, *109*.
- [8] Kwok, K. N.; Sze, S. M. *Physics of Semiconductor Devices*; Wiley Interscience, 2006; pp 16,17.
- [9] Direct and Indirect Band Gap Semiconductors. 2012; <https://www.doitpoms.ac.uk/tplib/semiconductors/direct.php>.
- [10] Saigal, N. Why do the PL spectra of indirect band gap semiconductor (for example Sb₂S₃) have to be tested at low temperatures? 2019.
- [11] Khare, A.; Wills, A. W.; Ammerman, L. M.; Norris, D. J.; Aydil, E. S. Size control and quantum confinement in Cu₂ZnSnS₄ nanocrystals. *Chem. Commun.* **2011**, *47*, 11721–11723.
- [12] Zwiller, V.; Blom, H.; Jonsson, P.; Panev, N.; Jeppesen, S.; Tsegaye, T.; Goobar, E.; Pistol, M.-E.; Samuelson, L.; Björk, G. Single quantum dots emit single photons at a time: Antibunching experiments. *Applied Physics Letters* **2001**, *78*, 2476–2478.
- [13] Migdall, A. *Single-photon generation and detection: physics and applications*; Academic Press, 2013; pp 42,44.
- [14] Bimberg, D.; Stock, E.; Lochmann, A.; Schliwa, A.; Tofflinger, J. A.; Unrau, W.; Munnix, M.; Rodt, S.; Haisler, V. A.; Toropov, A. I.; Bakarov, A.; Kalagin, A. K. Quantum Dots for Single- and Entangled-Photon Emitters. *IEEE Photonics Journal* **2009**, *1*, 58–68.
- [15] Patterson, J. D.; Bailey, B. C. *Solid-State Physics: Introduction to the Theory*; Springer, 2005; pp 615,621.
- [16] Tang, B.; Gong, L.; Hu, H.; Sun, H.; Zhou, S. Toward efficient long-wavelength III-nitride emitters using a hybrid nucleation layer. *Optics Express* **2021**, *29*, 27404.

BIBLIOGRAPHY

- [17] Li, J.; Yang, C.; Liu, L.; Cao, H.; Lin, S.; Xi, X.; Li, X.; Ma, Z.; Wang, K.; Patanè, A.; Zhao, L. High Responsivity and Wavelength Selectivity of GaN-Based Resonant Cavity Photodiodes. *Advanced Optical Materials* **2020**, *8*, 1901276.
- [18] Tamariz, S.; Callsen, G.; Stachurski, J.; Shojiki, K.; Butté, R.; Grandjean, N. Toward Bright and Pure Single Photon Emitters at 300 K Based on GaN Quantum Dots on Silicon. *ACS Photonics* **2020**, *7*, 1515–1522.
- [19] Tang, X.; Hu, Z.; Chen, W.; Xing, X.; Zang, Z.; Hu, W.; Qiu, J.; Du, J.; Leng, Y.; Jiang, X.; Mai, L. Room temperature single-photon emission and lasing for all-inorganic colloidal perovskite quantum dots. *Nano Energy* **2016**, *28*, 462–468.
- [20] Bayer, M. Bridging Two Worlds: Colloidal versus Epitaxial Quantum Dots. *Annalen der Physik* **2019**, *531*, 1900039.
- [21] Efros, A. L.; Nesbitt, D. J. Origin and control of blinking in quantum dots. *Nature Nanotechnology* **2016**, *11*, 661–671.
- [22] Nasilowski, M.; Spinicelli, P.; Patriarche, G.; Dubertret, B. Gradient CdSe/CdS Quantum Dots with Room Temperature Biexciton Unity Quantum Yield. *Nano Letters* **2015**, *15*, 3953–3958.
- [23] Javaux, C.; Mahler, B.; Dubertret, B.; Shabaev, A.; Rodina, A. V.; Efros, A. L.; Yakovlev, D. R.; Liu, F.; Bayer, M.; Camps, G.; Biadala, L.; Buil, S.; Quelin, X.; Hermier, J.-P. Thermal activation of non-radiative Auger recombination in charged colloidal nanocrystals. *Nature Nanotechnology* **2013**, *8*, 206–212.
- [24] Efros, A. L.; Nesbitt, D. J. Origin and control of blinking in quantum dots. *Nature Nanotechnology* **2016**, *11*, 661–671.
- [25] Hohng, S.; Ha, T. Near-Complete Suppression of Quantum Dot Blinking in Ambient Conditions. *Journal of the American Chemical Society* **2004**, *126*, 1324–1325.
- [26] Brown, R. H.; Twiss, R. Q.; Lovell, A. C. B.; surName, g. Interferometry of the intensity fluctuations in light - I. Basic theory: the correlation between photons in coherent beams of radiation. *Proceedings of the Royal Society of London. Series A. Mathematical and Physical Sciences* **1957**, *242*, 300–324.
- [27] Wikipedia, the free encyclopedia, Hanbury Brown and Twiss effect. 2020; https://en.wikipedia.org/wiki/Hanbury_Brown_and_Twiss_effect#/media/File:Correlation-interferometer.svg.
- [28] Eisaman, M. D.; Fan, J.; Migdall, A.; Polyakov, S. V. Invited Review Article: Single-photon sources and detectors. *Review of Scientific Instruments* **2011**, *82*, 071101.
- [29] Shields, A. J. Semiconductor quantum light sources. *Nature Photonics* **2007**, *1*, 215–223.
- [30] Northup, T. E.; Blatt, R. Quantum information transfer using photons. *Nature Photonics* **2014**, *8*, 356–363.
- [31] Thin Lens Equation. 2019; https://phys.libretexts.org/Courses/University_of_California_Davis/UCD%3A_Physics_7C_-_General_Physics/09%3A_Optics/9.3%3A_Lenses/9.3.3%3A_The_Thin_Lens_Equation.

BIBLIOGRAPHY

- [32] Lauterbach, M. A. Finding, defining and breaking the diffraction barrier in microscopy – a historical perspective. *Optical Nanoscopy* **2012**, *1*, 8.
- [33] Lund-Hansen, T.; Stobbe, S.; Julsgaard, B.; Thyrrestrup, H.; Sünder, T.; Kamp, M.; Forchel, A.; Lodahl, P. Experimental Realization of Highly Efficient Broadband Coupling of Single Quantum Dots to a Photonic Crystal Waveguide. *Phys. Rev. Lett.* **2008**, *101*, 113903.
- [34] Luxmoore, I. J.; Wasley, N. A.; Ramsay, A. J.; Thijssen, A. C. T.; Oulton, R.; Hugues, M.; Fox, A. M.; Skolnick, M. S. Optical control of the emission direction of a quantum dot. *Applied Physics Letters* **2013**, *103*, 241102.
- [35] Waveguide modes: TE, TM, TEM. 2016; <https://www.electronics-notes.com/articles/antennas-propagation/rf-feeders-transmission-lines/waveguide-modes-te-tm-tem.php>.
- [36] Flaviis, F. D. In *The Electrical Engineering Handbook*; CHEN, W.-K., Ed.; Academic Press: Burlington, 2005; pp 539–551.
- [37] Understanding Modal Propagation in Rectangular Waveguides. 2022; <https://resources.system-analysis.cadence.com/blog/msa2021-understanding-modal-propagation-in-rectangular-waveguides>.
- [38] Thorlabs resolution test targets. https://www.thorlabs.com/newgroupage9.cfm?objectgroup_id=4338&pn=R3L3S1P#.
- [39] Frazer, L.; Higginbotham, H. F.; Bell, T. D. M.; Funston, A. M. “It’s Fundamental”: Quantum Dot Blinking Experiment to Teach Critical Thinking. *Journal of Chemical Education* **2020**, *97*, 244–252.
- [40] Mahler, B.; Spinicelli, P.; Buil, S.; Quelin, X.; Hermier, J.-P.; Dubertret, B. Towards non-blinking colloidal quantum dots. *Nature Materials* **2008**, *7*, 659–664.
- [41] Chen, Y.; Vela, J.; Htoon, H.; Casson, J. L.; Werder, D. J.; Bussian, D. A.; Klimov, V. I.; Hollingsworth, J. A. “Giant” Multishell CdSe Nanocrystal Quantum Dots with Suppressed Blinking. *Journal of the American Chemical Society* **2008**, *130*, 5026–5027, PMID: 18355011.
- [42] Qin, W.; Shah, R. A.; Guyot-Sionnest, P. CdSeS/ZnS Alloyed Nanocrystal Lifetime and Blinking Studies under Electrochemical Control. *ACS Nano* **2012**, *6*, 912–918, PMID: 22191620.
- [43] Badri, S. H.; Gilarlue, M. Maxwell’s fisheye lens as efficient power coupler between dissimilar photonic crystal waveguides. *Optik* **2019**, *185*, 566–570.
- [44] Zwiller, V.; Aichele, T.; Seifert, W.; Persson, J.; Benson, O. Generating visible single photons on demand with single InP quantum dots. *Applied Physics Letters* **2003**, *82*, 1509–1511.
- [45] White, A. G.; Mitchell, J. R.; Nairz, O.; Kwiat, P. G. “Interaction-free” imaging. *Phys. Rev. A* **1998**, *58*, 605–613.
- [46]

BIBLIOGRAPHY

- [47] Masud, A. A.; Arefin, S. M. N.; Fairooz, F.; Fu, X.; Moonschi, F.; Srijanto, B. R.; Neupane, K. R.; Aryal, S.; Calabro, R.; Kim, D.-Y.; Collier, C. P.; Chowdhury, M. H.; Richards, C. I. Photoluminescence Enhancement, Blinking Suppression, and Improved Biexciton Quantum Yield of Single Quantum Dots in Zero Mode Waveguides. *The Journal of Physical Chemistry Letters* **2021**, *12*, 3303–3311.
- [48] Holmes, M. J.; Arita, M.; Arakawa, Y. III-nitride quantum dots as single photon emitters. *Semiconductor Science and Technology* **2019**, *34*, 033001.
- [49] Utzat, H.; Sun, W.; Kaplan, A. E. K.; Krieg, F.; Ginterseder, M.; Spokoyny, B.; Klein, N. D.; Shulenberger, K. E.; Perkinson, C. F.; Kovalenko, M. V.; Bawendi, M. G. Coherent single-photon emission from colloidal lead halide perovskite quantum dots. *Science* **2019**, *363*, 1068–1072.
- [50] Shalaginov, M. Y.; Vorobyov, V. V.; Liu, J.; Ferrera, M.; Akimov, A. V.; Lagutchev, A.; Smolyaninov, A. N.; Klimov, V. V.; Irudayaraj, J.; Kildishev, A. V.; Boltasseva, A.; Shalaev, V. M. Enhancement of single-photon emission from nitrogen-vacancy centers with TiN/(Al,Sc)N hyperbolic metamaterial. *Laser & Photonics Reviews* **2015**, *9*, 120–127.
- [51] Bouwmeester, D.; Ekert, A.; Zeilinger, A. *The Physics of Quantum Information*; Springer, 2000.